



Polymerization of isatin towards polymers for anion exchange membranes and gas separation applications

SIMONE FACCHINI | CENTRE FOR ANALYSIS AND SYNTHESIS | LUND UNIVERSITY

Supervisor: Dong Pan

Examiner: Professor Patric Jannasch



LUND UNIVERSITY

Abstract

In a world where the problem of energy resources, pollution and all aspects related to these issues becomes more and more dominant, a greater commitment is needed in the search for solutions. The goal of this project is to make a contribution to the research and development of new materials to reduce the environmental impact in some fields. First of all, we tried to synthesize and prepare an isatin-based membrane which has the potential for use in separating industrial gases. Furthermore, ion exchange membranes, specifically hydroxide exchange membranes (HEMs) derived from the same material were developed for fuel cells (HEMFC) applications. These materials are essential for energy conversion and storage. The most difficult challenge is to guarantee their thermal stability and stability in corrosive environments such as alkali without losing efficiency. In recent years the polyhydroxyalkylation catalysed with superacids, e.g. TFSA, has become increasingly studied. This reaction is exploited for the synthesis of the compounds of this thesis. After a preliminary optimization of the reaction conditions it was concluded that, due to the rigidity and excessive reactivity of the monomers, it was not possible to obtain the isatin-based membrane to evaluate the gas separation properties. The synthesis of precursor materials for HEMs was successful. Instead of isatin, 1-(4-bromobutyl)indoline-2,3-dione (BID) was used as a substitute. A characterization of the polymers was carried out using NMR, TGA and DSC analyses, and subsequently the membranes were functionalized with different ammonium-based cations. Unfortunately, this last step was not successful due to the appearance of side reactions. Future studies on the mechanism and kinetics of the reaction may solve this obstacle.

I en värld där problemet med energiresurser, föroreningar och alla aspekter relaterade till dessa frågor blir mer och mer dominerande behövs ett större engagemang i sökandet efter lösningar. Målet med detta projekt är att ge ett bidrag till forskning och utveckling av nya material, för att minska miljöpåverkan inom vissa områden. Först och främst försökte vi syntetisera och framställa ett isatinbaserat membran som har potential att användas för att separera industrigaser. Vidare utvecklades jonbytarmembran, speciellt hydroxidutbytesmembran (HEM) härledda från samma material för bränslecellstillämpningar (HEMFC). Dessa material är avgörande för energiomvandling och lagring. Den svåraste utmaningen är att garantera deras termiska stabilitet och stabilitet i korrosiva miljöer som alkali utan att förlora effektivitet. På senare år är katalyserade polyhydroxialkyleringar med supersyror, t.ex. TFSA, har blivit alltmer studerad. Denna reaktion utnyttjas för syntes av föreningarna i denna avhandling. Efter en preliminär optimering av reaktionsbetingelserna drogs slutsatsen att på grund av isatins styvhet och höga reaktivitet var det inte möjligt att erhålla det isatinbaserade membranet för att utvärdera gasseparationsegenskaperna. Syntesen av prekursor material för HEM var framgångsrik. Istället för isatin användes 1-(4-bromobutyl)indolin-2,3-dion (BID) som ett substitut. En karakterisering av polymererna utfördes med NMR-, TGA- och DSC-analyser, och därefter funktionaliserades membranerna med olika ammoniumbaserade katjoner. Tyvärr var detta sista steg inte framgångsrikt på grund av bireaktioner. Framtida studier av reaktionens mekanism och kinetik kan lösa detta hinder.

In un mondo in cui il problema delle risorse energetiche, dell'inquinamento e di tutti gli aspetti legati a questi temi diventa sempre più dominante, è necessario un maggiore impegno nella ricerca di soluzioni. L'obiettivo di questo progetto è dare un contributo alla ricerca e sviluppo di materiali per diminuire l'impatto ambientale in alcuni campi molto utilizzati ai giorni nostri. Come prima cosa si è cercato di sintetizzare una membrana a base di isatina che si suppone abbia buone performance per una separazione dei gas industriali più utilizzati. Successivamente lo scopo è quello di sviluppare membrane a scambio ionico da utilizzare nelle celle a combustibile (HEMFC), nello specifico membrane a scambio di idrossidi (HEM). Questi materiali sono essenziali per la conversione e lo stoccaggio dell'energia. La sfida più difficile attualmente è garantire la loro stabilità termica e quella in ambienti corrosivi come quelli alcalini senza perdere di efficienza. Negli ultimi anni la polioidrossialchilazione catalizzata con superacidi, ad es. TFSA, è diventato sempre più studiato. Questa reazione viene sfruttata per la sintesi dei composti di questa tesi. Dopo una preliminare ottimizzazione delle condizioni di reazione si è concluso che a causa della rigidità e dell'eccessiva reattività del sistema, non era possibile ottenere la membrana a base di isatina per valutare le proprietà di separazione dei gas. La sintesi di materiali precursori per gli HEM ha avuto successo. Al posto dell'isatina, come sostituto è stato utilizzato 1-(4-bromobutil)indolina-2,3-dione (BID). È stata effettuata una caratterizzazione dei polimeri mediante analisi NMR, TGA e DSC e successivamente le membrane sono state funzionalizzate con diversi cationi a base di ammonio. Sfortunatamente, quest'ultimo passaggio non ha avuto successo a causa di reazioni collaterali. Studi futuri sul meccanismo e sulla cinetica della reazione possono essere utilizzati per risolvere questo ostacolo.

Table of contents

Abstract	2
Table of contents.....	5
Abbreviations.....	7
Popular science summary	8
1 Approach and aim.....	10
2 Introduction.....	13
2.1 Fuel cells	13
2.1.1 Proton-exchange membrane fuel cells.....	13
2.1.2 Alkaline fuel cells.....	14
2.1.3 Hydroxide exchange membranes fuel cells	14
2.1.4 Properties of HEMs:	15
2.1.5 Polymer backbone:.....	17
2.1.6 Cations:	19
2.2 Free Volume Theory.....	23
2.3 Gas separation.....	25
2.4 Polymerization and mechanism	26
2.5 Characterization methods.....	29
2.5.1 Size exclusion chromatography (SEC)	29
2.5.2 Thermal gravimetric analysis (TGA)	32
2.5.3 Differential scanning calorimetry (DSC)	32
2.5.4 Water uptake	33
2.5.5 Ion exchange capacity (IEC)	33
2.5.6 Hydroxide Conductivity	34
2.5.7 Alkaline stability.....	35
3 Experimental methods.....	36
3.1 Monomer synthesis	36
3.2 Synthesis of PSIX.....	37
3.3 Synthesis of PBSIX	38
3.4 Polymer modification and functionalization.....	39
3.5 Membrane preparation.....	40
4 Results and Discussion.....	41
4.1 Monomer characterizations.....	41

4.1.1	Isatin	41
4.1.2	BID	42
4.2	Polymer characterizations	45
4.2.1	PSIX	45
4.2.2	PBSIX	49
4.3	Quaternization	51
4.4	Reaction mechanism	54
4.5	Membrane characterizations	57
4.6	SEC	59
4.7	TGA and DSC	60
5	Conclusion and future outlook	63
6	References	65
7	Acknowledgements	74

Abbreviations

AEM	anion exchange membrane
AEMFC	anion exchange membrane fuel cell
AFC	alkaline fuel cell
BID	1-(4-bromobutyl)indoline-2,3-dione
DCM	dichloromethane
DMSO	dimethylsulfoxide
FC	fuel cell
HEM	hydroxide exchange membrane
HEMFC	hydroxide exchange membrane fuel cell
IEC	ion exchange capacity
IEM	ion-exchange membrane
NMP	<i>N</i> -methyl-2-pyrrolidone
PSIX	poly (2',7'-spiro[indoline-3,9'-xanthen]-2-one)
PBSIX	poly (1-(4-bromobutyl)-2',7'-spiro[indoline-3,9'-xanthen]-2-one)
PEM	proton exchange membrane
PEMFC	proton exchange membrane fuel cell
QA	quatarnary ammonium
SGP	step-growth polymerization
TFA	trifluoroacetic acid
TFSA	trifluoromethanesulfonic acid
TMA	trimethylamine

Popular science summary

It is no secret that one of the biggest problems of modern times is climate change. This topic has been avoided for many generations and in recent years all industries and the world of marketing have begun to move and raise awareness on this issue. There is already much evidence that links the connection between man-caused damage to the environment and increasingly frequent natural disasters. The increase in temperature due to the accumulation of carbon dioxide in the atmosphere has not only impacted the climate but also the life cycle of the animals. Related to that it is estimated that some species have been forced to change the place where they generally resided and move closer near inhabited centres, bringing new contacts and the onset of new diseases. The solution being adopted is the search for renewable energy sources such as solar, hydrogen and bio fuels, and the development of new technologies green-energy based. However, compounds such as membranes, capable of energy converting economically and efficiently, must support these technologies.

One of the most energy-intensive industrial processes is the selective separation of the components of a gas or a liquid gas stream. The classic methods such as extraction, distillation and absorption are essential and not very green. For this reason, an alternative solution was sought. The separation of gas mixtures employing polymeric membranes has been commercially utilized since the late 1970s. While the ability to separate gas mixtures was recognized much earlier, the commercial reality has only recently generated a significant amount of academic and industrial research activity. Membrane separation has many advantages such as low energy consumption, economy and versatility. Another area of emerging importance for these materials is the recapture of CO₂ from industrial processes. For these reasons, we have in this work tried to design an isatin-based membrane for this purpose. There are various problems in the synthesis mechanism that did not allow control over the product structure. What was supposed to be a flexible film turned out to be fragile and of low quality and therefore unusable as it was initially thought.

The other field that this work was aimed at is that of fuel cells. Briefly, these are electrochemical devices that allows to obtain electrical energy directly from certain substances, typically from hydrogen, without any thermal combustion process-taking place. Between the anode and cathode there must be a means of connection between the two parts. Generally, this connection is composed of a liquid, but many polymeric membranes that can replace them are being studied. In our specific case, we are talking about anion exchange membranes (AEM),

consisting of a neutral polymeric backbone to which positively charged chemical groups are attached. These, generally quaternary ammonium salts (QA), are responsible for the transport of anions, and therefore of the current, inside the batteries or fuel cells. In this project, a less reactive isatin derivative was synthesized and polymerized. The membrane precursor had the same problem found in the first part of the study. In addition, this time a side reaction prevented the functionalization of the polymer. The usage of this polymer need a more in-depth analysis of the reaction mechanism.

To summarize, the work focus on two main topics, the synthesis of a gas separation membrane and an AEM. The successful optimization of the reaction conditions led to obtaining the polymeric compounds. The quality of the isatin polymer films were brittle and not enough to provide films for gas separation characterizations. The functionalization reaction of the polymer for AEMs was unsuccessful. The thermal and structure characterization using TGA and NMR analysis had provided a likely explanation about the reasons of the problems encountered.

1 Approach and aim

In this thesis we investigated the polymerization of a monomer containing a carbonyl group (electrophile) and a nucleophile. The electron-rich molecule is 4,4'-dihydroxybiphenyl (*a*). The hydroxyl substituents activate the aromatic ring permit electrophilic substitution reactions. The reactive positions of the ring are *-para*, already occupied, and *-ortho*. Two electrophiles were used: isatin (*b*) and 1-(4-bromobutyl)indoline-2,3-dione (BID) (*c*). While isatin and 4,4'-dihydroxybiphenyl are easily available and at low cost, BID was synthesized. In **Figure 1.1** the molecular structure of the three monomers is shown.

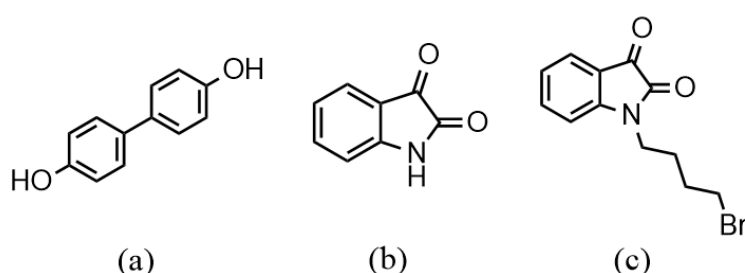


Figure 1.1 Molecular structure of 4,4'-dihydroxybiphenyl (*a*); isatin (*b*); 1-(4-bromobutyl)indoline-2,3-dione (*c*).

The first polymer was denoted poly(2',7'-spiro[indoline-3,9'-xanthen]-2-one) (PSIX), and the synthetic route is shown in **Figure 1.2**. The aim was to design and synthesize of a membrane with gas separation properties. This was because membranes are the greenest solution with the lowest environmental footprint to the problem of energy-intensive processes such as gas separations, air separation, hydrogen recycle, natural gas sweetening, and CO₂ capture and sequestration, on an industrial scale. The toughest challenges are to reach high selectivity and gas permeability, while maintaining good mechanical properties and low cost of production.

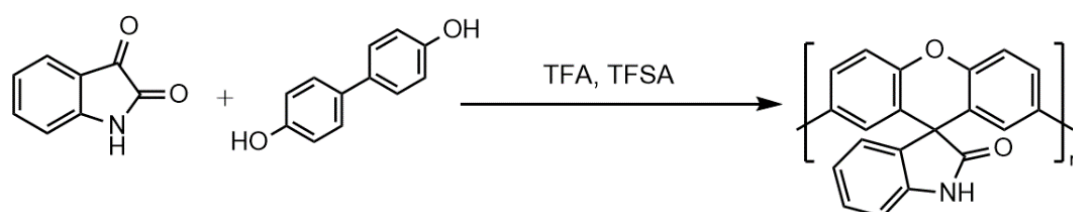


Figure 1.2 Synthesis of PSIX.

The gas separation properties were related to the conformation that the polymer assumes in 3D space. The polymer backbone was thought to be very rigid and with limited free volume. A 3D schematic is shown in **Figure 1.3**.

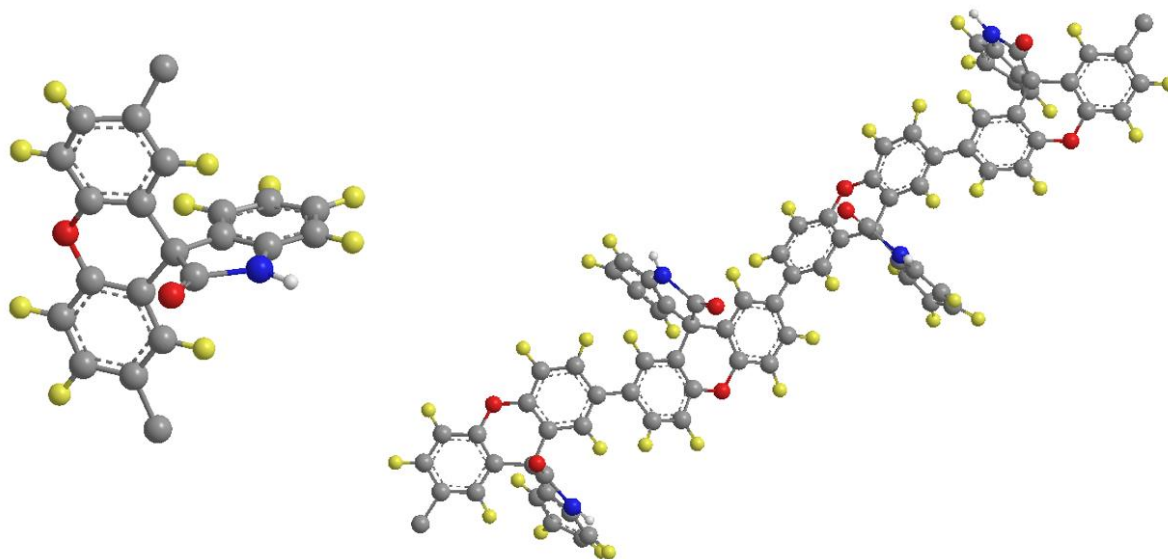


Figure 1.3 3D structure of PSIX.

The second aim of this thesis was to prepare hydroxide exchange membrane (HEM), employing the polymer described below. These membranes are very important for energy storage and for the use as solid electrolytes to replace, e.g., alkaline aqueous solutions in fuel cells.

The precursor polymer of the membranes was the PBSIX [poly(1-(4-bromobutyl)-2',7'-spiro[indoline-3,9'-xanthen]-2-one)], formed by polymerization of BID and 4,4'-dihydroxybiphenyl. **Figure 1.4 (a)** shows the synthesis pathways to obtain BID, while **Figure 1.4 (b)** shows the conditions for the synthesis of PBSIX.

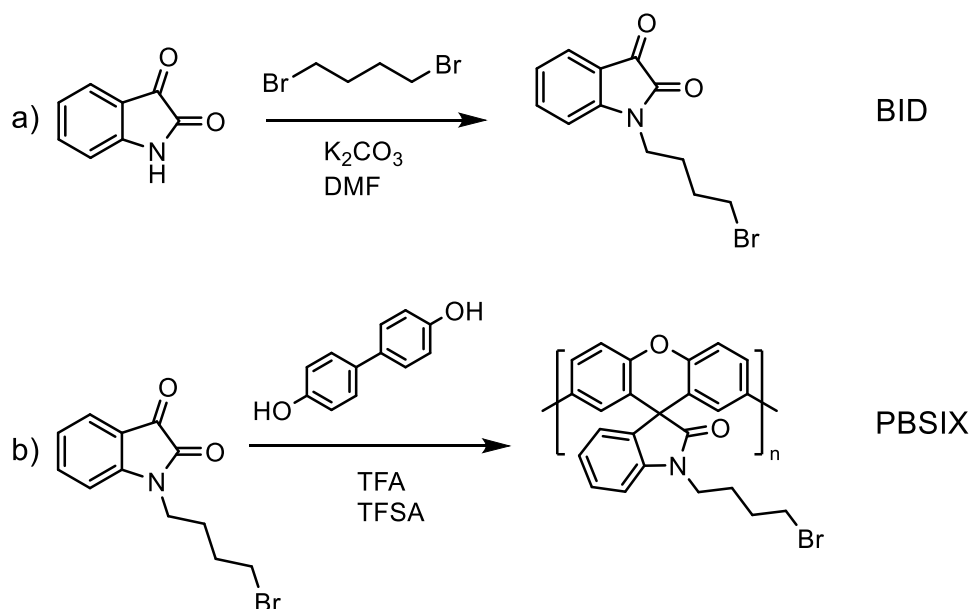


Figure 1.4 Synthesis of BID (a) and PBSIX (b).

Also in this case a 3D image of the polymer was provided (**Figure 1.5**). The alkyl chain will increase the free volume and the resulting polymer will be less suitable for gas separation applications.

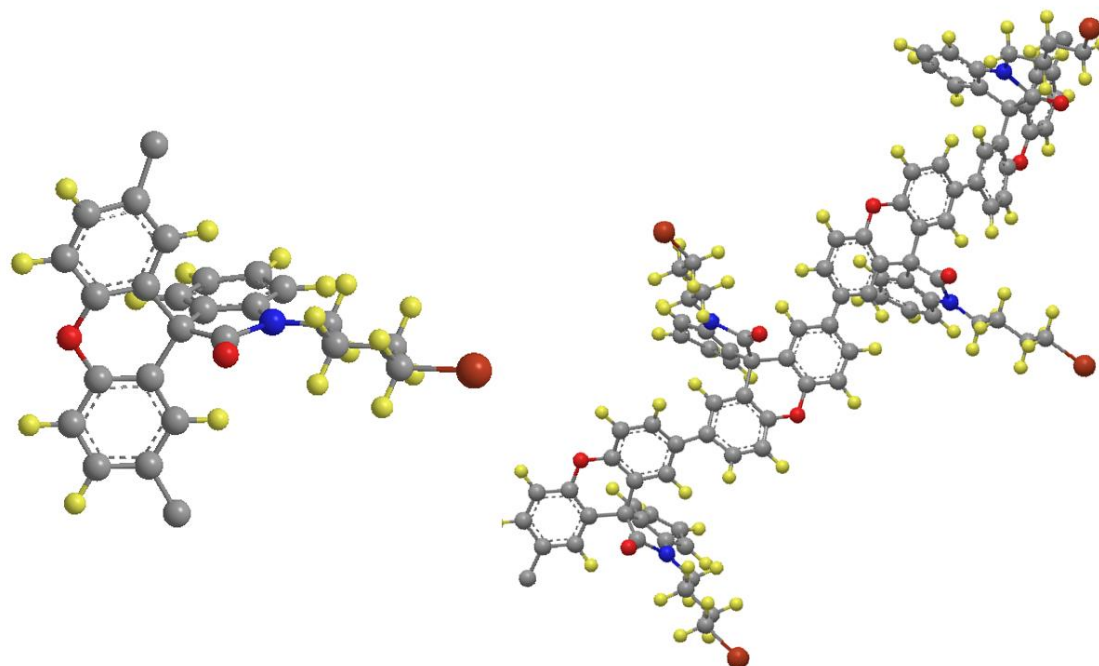


Figure 1.5 3D structure of PBSIX.

To obtain the HEMs, a functionalization of the polymers was necessary. To prepare anionic exchange membranes, quaternary ammonium (QA) cations were inserted along the polymer chain. The QAs chosen were trimethylamine (TMA), *N*-methylpiperidine (Pip) and *N*-methylpyrrolidine (Pyr) (**Figure 1.6**).

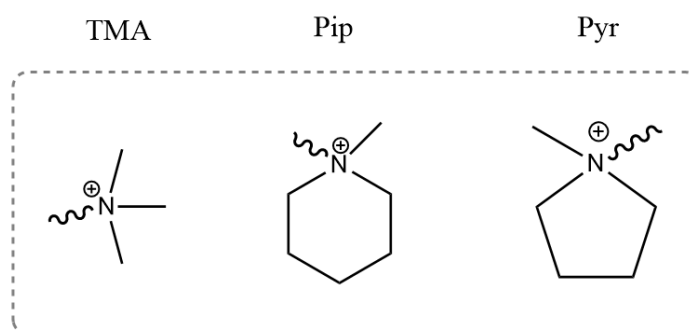


Figure 1.6 QA cations for HEMs.

After obtaining the functionalized membranes, characterizations with regard to water uptake, ion exchange capacity (IEC), conductivity and alkaline stability were planned.

2 Introduction

This chapter briefly summarizes all the knowledge useful for understanding the thesis work.

2.1 Fuel cells

A fuel cell (FC) is an electrochemical system in which the chemical free energy of a gas or a liquid is continuously converted to electrical energy via redox reactions.⁴ Similar to a battery, an FC is also made of two electrodes called anode and cathode, separated by an electrolyte. Oxidation occurs at the anode, while reduction at the cathode. These devices can be divided according to the type of the electrolyte used. Proton-exchange membrane fuel cells (PEMFCs), alkaline fuel cells (AFCs) and hydroxide exchange membrane fuel cells (HEMFCs) will be briefly discussed below. **Figure 2.1** shows a general scheme of operation conditions of polymeric based fuel cells.

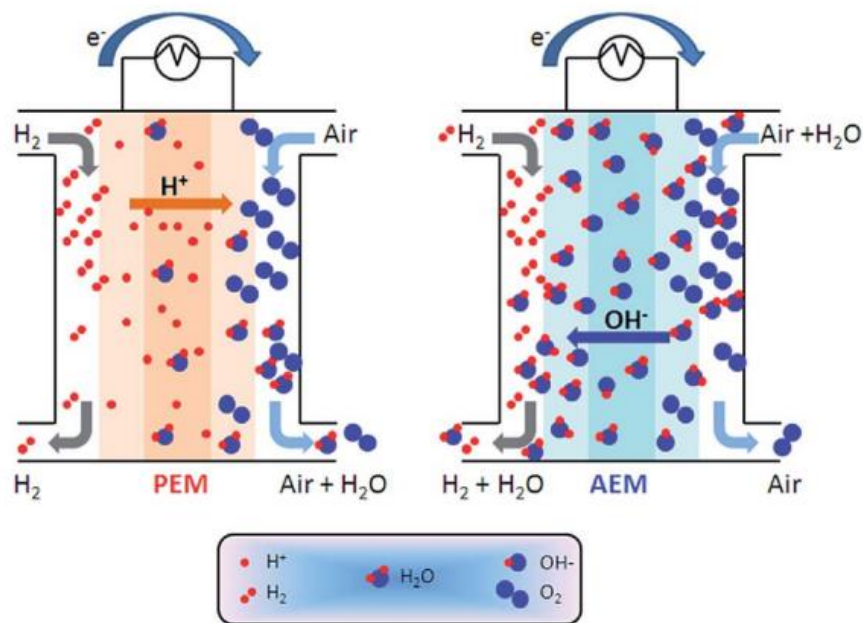
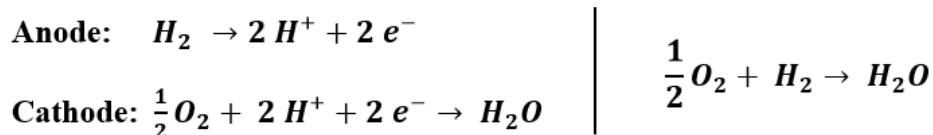


Figure 2.1 Schematic comparison of a PEMFC (left) and an AEMFC (right).³⁴

2.1.1 Proton-exchange membrane fuel cells

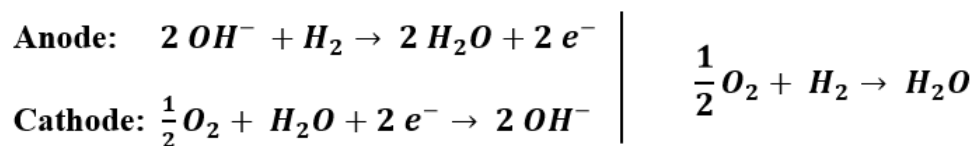
In this type of FC the electrolyte is a proton exchange membrane (PEM).²¹ The electrochemical reactions that take place in a PEMFC are the following:



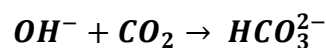
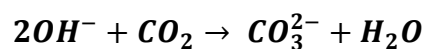
Due to the limitations of PEMs, the temperature range of use of PEMFCs is restricted to between 50 to 100 °C⁴ (water use limit temperature). At these temperatures the electrochemical reactions are slow, and for this reason it is necessary to use expensive metals, such as platinum, as catalysts.⁶ One of the most commonly used PEMs today is Nafion[®], developed already in the 1960s by DuPont.⁷ It is a copolymer consisting of a Teflon-based backbone with perfluorinated sidechains terminated with sulfonic acid groups.

2.1.2 Alkaline fuel cells

One of the earliest FC developed was the AFC.^{28,29} It works by using an alkaline solution of KOH as electrolyte.^{5,8} The electrochemical reactions in alkaline media are:



One of the advantages of a high pH environment is that the electrochemical reactions are faster, thanks to a kinetic aid. This allows to replace the use of platinum with cheaper metals such as Co, Ag and Fe.^{9,30-35} There are two main disadvantages to consider. Foremost, a hot alkaline solution of OH⁻ is highly corrosive; there is a risk for both human safety and machinery to be damaged. Furthermore, the electrodes are subjected to poisoning caused by CO₂ in the air which decreases their efficiency.



The hydroxide ions are consumed by the CO₂ forming carbonates and causing a decrease in the current generated. These carbonates, in turn, create salts with K⁺ ions. Once precipitated, these salts block the electrodes and prevent the gas diffusion.

2.1.3 Hydroxide exchange membranes fuel cells

In recent decades a new fuel cell system in an alkaline environment has been studied.¹⁰ It is called hydroxide exchange membrane fuel cell (HEMFC). This type of membrane belongs to the large group of Ion Exchange Membrane (IEM). HEMs typically consist of a hydrophobic polymer as backbone functionalized with ionic groups and their counter-ions.¹² The osmotic pressure causes an absorption of water inside the membrane, which allows a partial dissociation of the counter-ions and their diffusion through the material. HEMs have found use in several

applications related to energy conversion and storage; the most common are reverse electrodialysis,¹³ and water electrolysis¹⁷. What makes the use of HEM interesting is the fact that this system combines the advantages of PEMFCs and the AFCs.^{9,34} Reactions are kinetically promoted and the electrolyte is solid, making the device safer.¹⁹ Typically, the most used cations are quaternary ammonium groups (QA).²⁰ In the next section we will discuss the properties that affect the quality of HEMs.

2.1.4 Properties of HEMs:

The properties and fundamental requirements of an HEM are:

- High hydroxide conductivity
- High mechanical, thermal and chemical stability against radicals, bases and nucleophiles
- Good gas permeability and separation properties

The ion exchange capacity (IEC) is the parameter to consider when determine the efficiency and capacity (in terms of power density) of the fuel cell. One of the differences between PEMs and HEMs is the transported ion from H^+ to OH^- . This introduces some obstacles to overcome. First, the diffusion coefficient and ionic mobility of H^+ in water compared to OH^- are intrinsically higher,⁴⁵ thanks to a smaller size and solvation capacity;⁴⁴ the reason why these ions are so mobile compared to others is due to the latter's diffusion mechanism. According to the Grotthuss mechanism (**Figure 2.2**),⁴³ the phenomenon is interpreted as a defect in the O-H bonds in the liquid.⁴² In addition, QA dissociation is less than the PEMs sulfonic acid groups. Both factors decrease the ion conductivity.

Secondly, we have to consider the alkaline stability^{37,61,62} of the polymer in a nucleophilic and basic environment. While the activity of H^+ towards the polymer is very low, OH^- can react both with the organic molecules of the polymer and with functional groups that can act as leaving groups in several organic reactions of elimination.

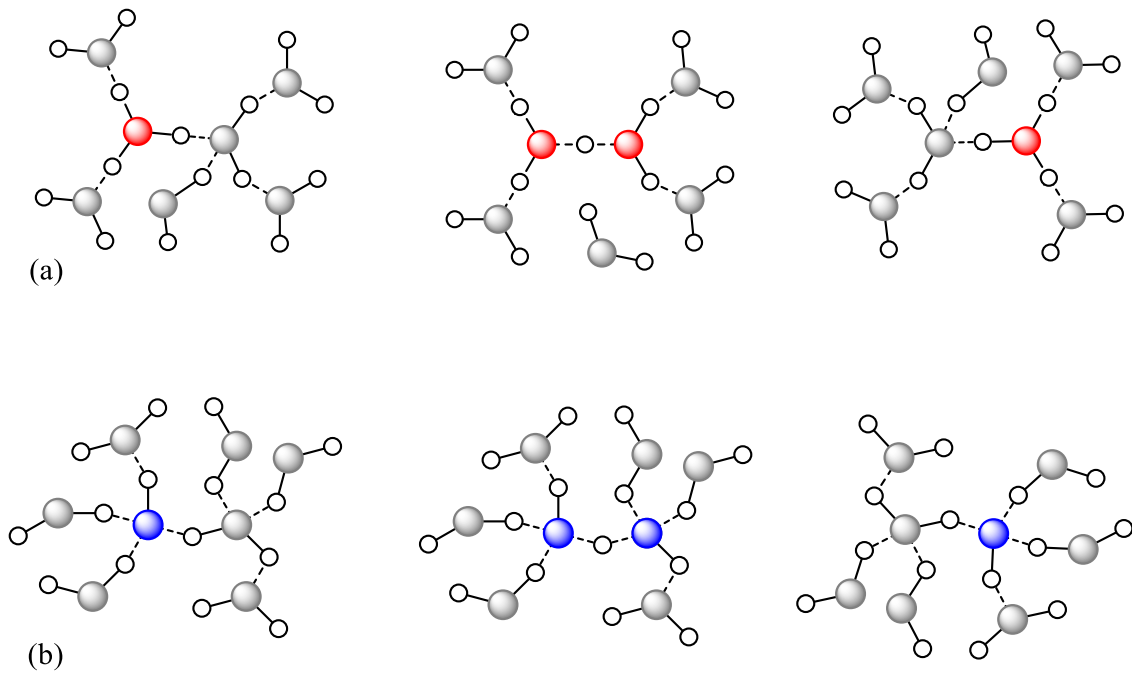


Figure 2.2 Structural diffusion of (a) proton and (b) hydroxide ions.

The amount of water that a membrane absorbs is defined as water uptake. A water content is essential for the transport of ions; insufficient water uptake decreases the OH^- conductivity. Meanwhile, an excess of water will lead to a dilution effect, which can decrease the conductivity.^{39,46} Moreover, a high amount of water leads to an excessive swelling of the membrane, impairing the mechanical properties. The main risk is the breaking of the membrane.⁴⁷

Thermal and chemical stability are directly related to the lifetime of the membrane in the fuel cell conditions. Increasing the temperature improves the conductivity, but stability problems will arise. Depending on the degree of solvation and the temperature, the degradation mechanisms and its ratio can vary.⁴¹ Some examples of degradation pathways are shown in **Figure 2.3**.

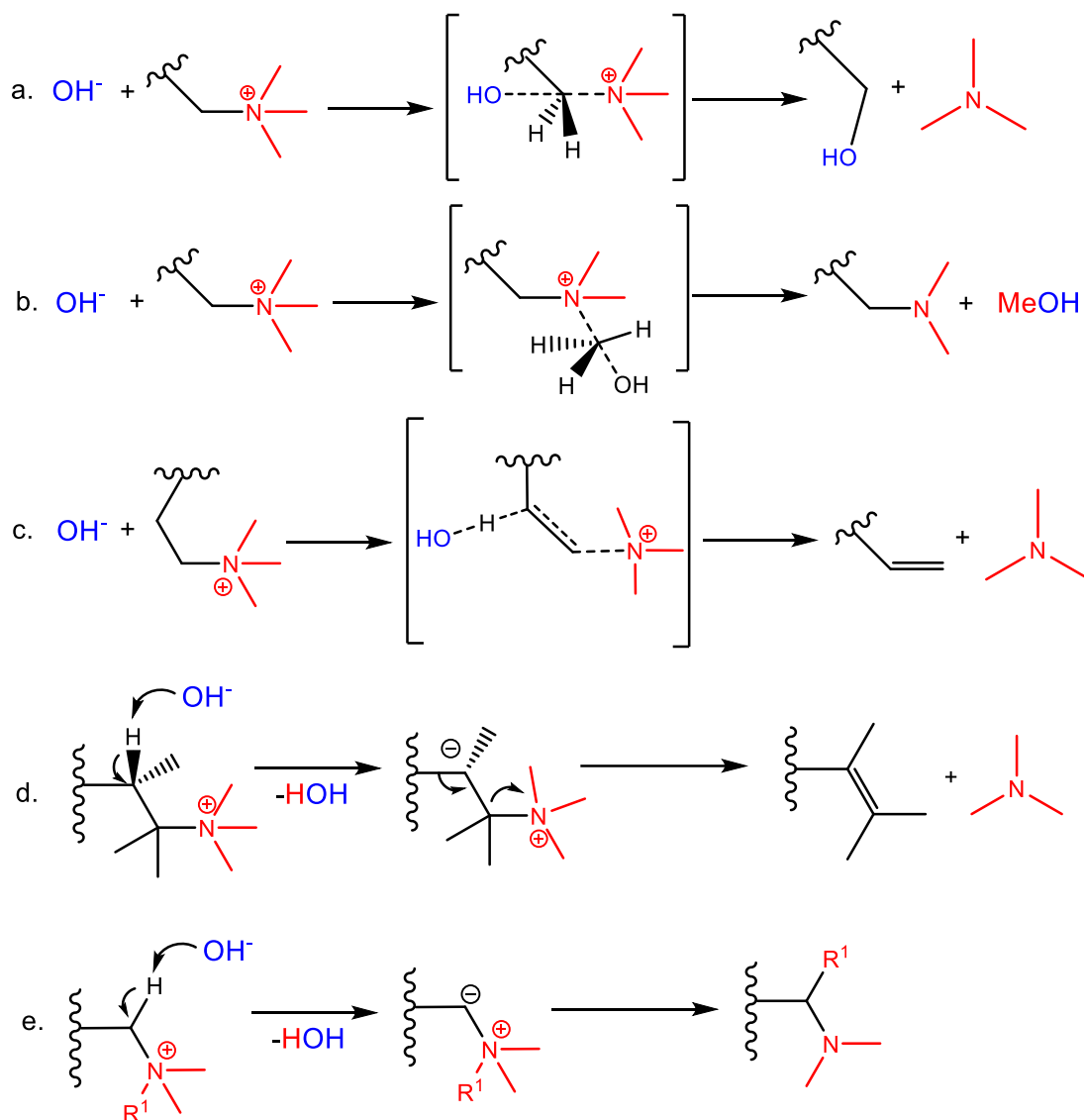


Figure 2.3 Degradation reactions of QA: nucleophilic substitution at benzyl (a) and methyl (b) positions, Hofmann elimination (E2) (c), E1cb elimination (d), and Stevens rearrangement (e).⁴¹

2.1.5 Polymer backbone:

The polymer backbone plays a fundamental role both in membrane chemical stability and in maintaining high mechanical properties. Furthermore, it has the function of avoiding a considerable difference in size due to swelling in aqueous medium. The chemical degradation of macromolecules leads to a decrease in molecular weight, with a high risk of membrane collapse. The most suitable backbones are those with high glass transition temperature (T_g) and mainly aromatic ones. In the history of HEM research, the main backbones used were based on polysulfone (PSU) and poly(p-phenylene oxide) (PPO), and their structure are shown in **Figure 2.4 (a)(b)**. These polymers had the advantage of having good film properties and easy functionalization in many ways.^{116,117} The biggest drawback, especially for PSUs, is poor alkaline stability.

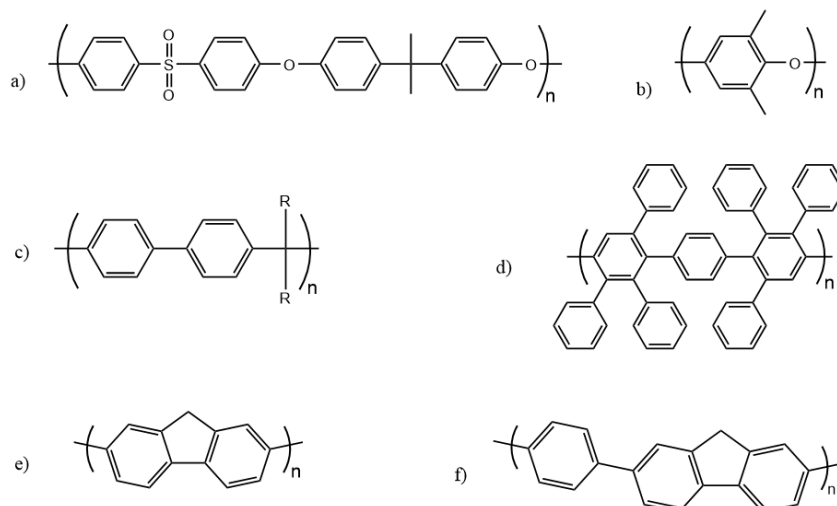


Figure 2.4 Example of HEMs backbones: polysulfone (PSU) (a), poly (*p*-phenylene oxide) (PPO) (b), poly(arylene alkylene) (PAA) (c), polyphenylenes (d), fluorene-based polymers (e)(f).

The ether bonds and quaternary carbons are most sensitive to degradation,⁵⁵⁻⁵⁹ with an increase in the rate of decomposition if the bond is in the vicinity of the QA. Under alkaline conditions these groups are activated for hydrolysis,¹¹⁸⁻¹²² which the mechanism is shown in **Figure 2.5**.

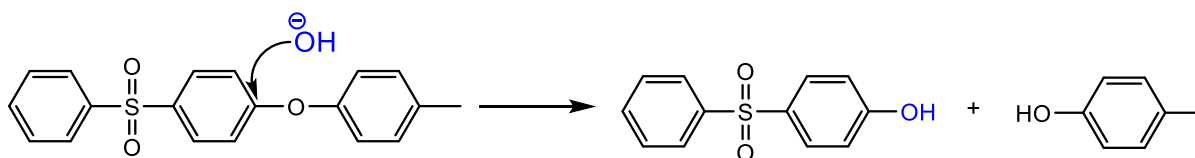


Figure 2.5 Degradation mechanism of a PSU in an alkaline media.

Deactivation strategies, including β -hydrogen-free cations, steric protection,⁶⁰⁻⁶² resonance and inductive effects,⁶³⁻⁷⁰ and conformational restriction¹²³⁻¹²⁷ can be employed to obtain more stable backbones. Thanks to different ways of synthesis ether-free backbones have been studied. Some examples are poly(arylene alkylene) (PAAs)¹³²⁻¹⁴⁰ shown in **Figure 2.4** (c), polyphenylenes^{130,131} (d) and fluorene-based polymers (e) (f).^{128,63}

The last aspect left to analyse is the choice of the cations. It should show alkaline stability properties, hydrophilic part, good oxidative and voltage stability.⁷¹ A balance has to be found between structural integrity and hydrophilicity, due to their inverse correlation.^{38,129,141} Lower hydrophilicity leads to decreased performance of the fuel cell, water uptake and IEC properties. An aspect that influences the alkaline stability is also the positioning of the cation along the polymer chain. **Figure 2.6** shows three main possible situations: in (a) the cation is incorporated in the chain; in (b) it is directly attached to the backbone; in the latter case (c) it is connected through a spacer. According to the experiments data, attaching cation groups to a polymer using hydrocarbon spacer chain has been shown to improve alkaline stability.^{143,144}

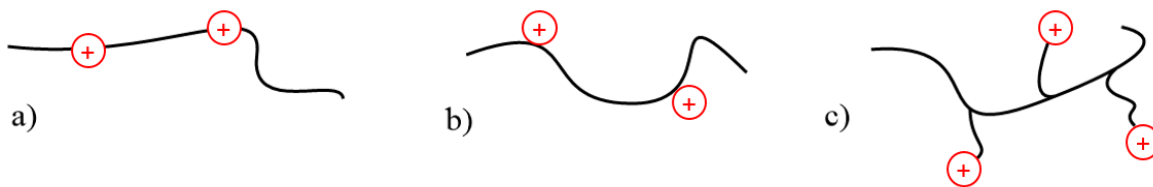


Figure 2.6 Examples of polymer cationic architectures.

2.1.6 Cations:

The main types of cations used in the HEMs development process are three:

- Ammonium-based
- Phosphonium and sulfonium-based
- Organic metal cation-based

Ammonium-based

Generally, the cations of this category are quaternary ammonium (QA) and imidazolium (IM) based. They are the most studied, this is due to their low cost and easy availability, but they are also the most prone to degradation with increasing in temperature and pH conditions.^{142,145-147} In particular, the reactions to which QAs are most sensitive are Hofmann elimination (E2),⁴⁸⁻⁵⁰ nucleophilic substitution (S_N2)^{36,51}, Stevens rearrangement⁵²⁻⁵⁴ and ring-opening. Elimination is mostly promoted by the presence of β -hydrogen via anti-coplanar step. A safe way to avoid the Hofmann degradation is the design of free β -hydrogens polymer.

In **Figure 2.7** some of the most used QA are classified according to the life time in alkaline conditions [6 M NaOH, 160 °C].³⁶

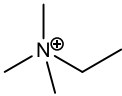
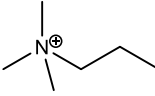
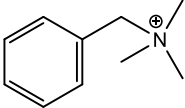
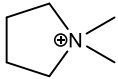
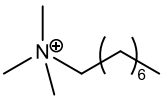
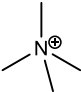
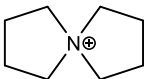
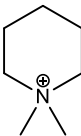
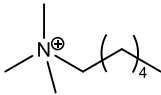
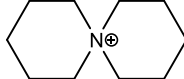
QA (Abbreviation)	Half-life [h]	QA (Abbreviation)	Half-life [h]
 ETM	2.8	 PTM	33.2
 BTMA	4.18	 DMPy	37.1
 OTM	12.7	 TMA	61.9
 ASD	28.4	 DMP	87.3
 HTM	31.9	 ASU	110

Figure 2.7. Half-lives of QA cations in 6 M NaOH at 160 °C.

The trend of the alkyl QA shows high stability of the trimethylamine, the almost non-existent stability of the ETM, and then the stability increases with the PTM. Benzyl QAs are unstable under alkaline conditions. *N*-Alicyclic QA groups were found to be the most stable.

Phosphonium and sulfonium-based

These cations, unlike QAs, have not been studied much. The reason is that these groups have considerably low thermal, chemical stability and low conductivity compared to their competitors.^{18,148-150} As can be seen in **Figure 2.8**, these groups are very sterically impeded, making hard the attach to the polymer.

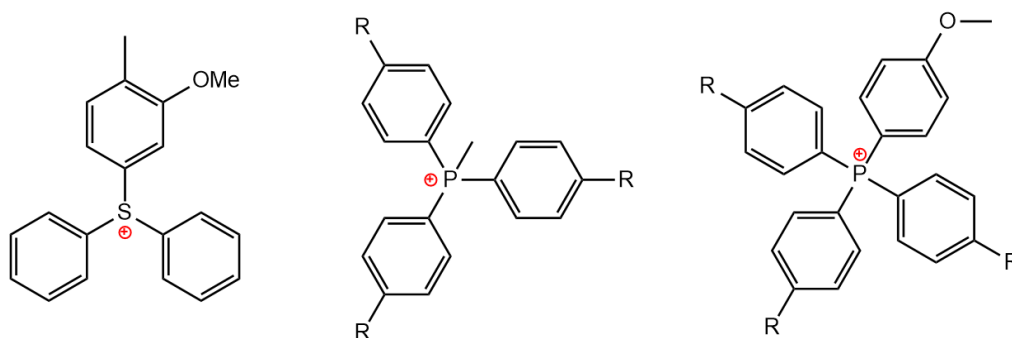


Figure 2.8 Phosphonium and sulfonium cation groups.

Organic metal cation-based

These cations are the most expensive to synthesize and require large ligands, as shown in **Figure 2.9**. Complexes of cobalt(I),^{152,153} ruthenium(II)¹⁵¹ and nickel(II)¹⁵⁴ were studied. Alkaline stability is strongly linked to the nature of the ligands. Electron-withdrawing group dramatically decreased their stability.

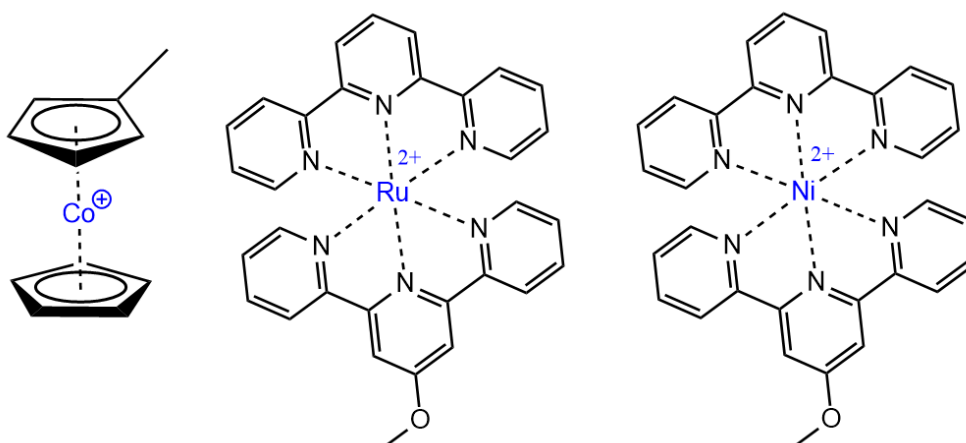


Figure 2.9 Organometallic cation groups.

In this work only QA cations were used. In particular, in **Figure 2.10** are shown alkyl-trimethylammonium (TMA) (a), alkyl *N*-methylpiperidinium (MPip) (b) and alkyl *N*-methylpyrrolidinium (MPyr) (c) are selected.

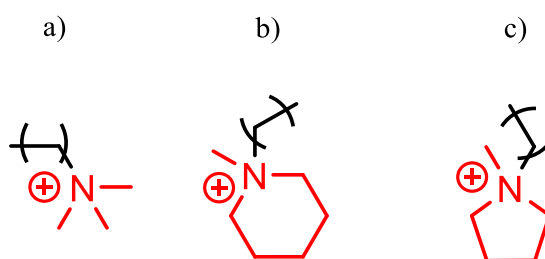


Figure 2.10 QAs chosen to functionalize HEMs.

In literature there are several studies in which the various degradation pathways of these compounds are analyzed. Starting with the N-cycles, the three main reactions considered are: (1) nucleophilic substitution, (2) ring-opening substitution, (3) ring-opening elimination (**Figure 2.11**). From the analysis of the products, it has been estimated that in the case of the 6-atom ring the predominant reaction is nucleophilic substitution. For the 5-atom ring, both reactions of nucleophilic substitution and ring-opening substitution are relevant. The ring-opening elimination becomes significant only considering n -atom rings with $n \geq 7$.^{36,155-157}

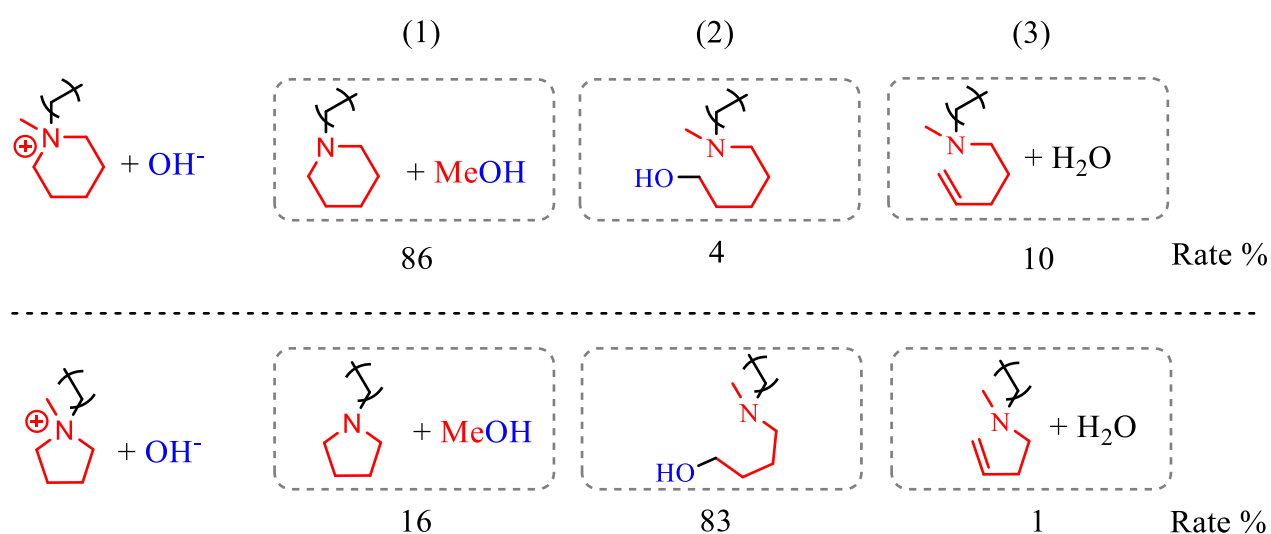


Figure 2.11 Degradation pathways of MPip and MPyr under alkaline conditions.

Observing the life times of these cations presented in **Figure 2.7**, we notice that they are much higher than what can be expected. These rings have many β -hydrogens (**Figure 2.12 (I)**) and as the temperature increases, ring-opening elimination should be the dominant one.^{158,159} To explain this resistance to elimination, two aspects must be considered: to begin with, the ring tension that prevents free rotation must be taken into consideration. In addition, it is significant to analyse the stability of the intermediate that is created in the elimination mechanism. In **(II)** is depicted the nucleophilic substitution mechanism in which the trigonal bipyramidal transition state does not require great distortion angles to occur, leading to be the dominant reaction. In the ring-opening substitution **(III)**, these angles can only be acquired through distortion of the 6-membered ring and this restriction limits the rate of this reaction. As shown in **(IV)**, the transition state for the ring-opening elimination requires energetically expensive bond angles and lengths which become acceptable only as the number of atoms composing the cycle increases. We can conclude that the balance between ring strain and transition-state energy determines which of the three possible degradation pathways predominates.

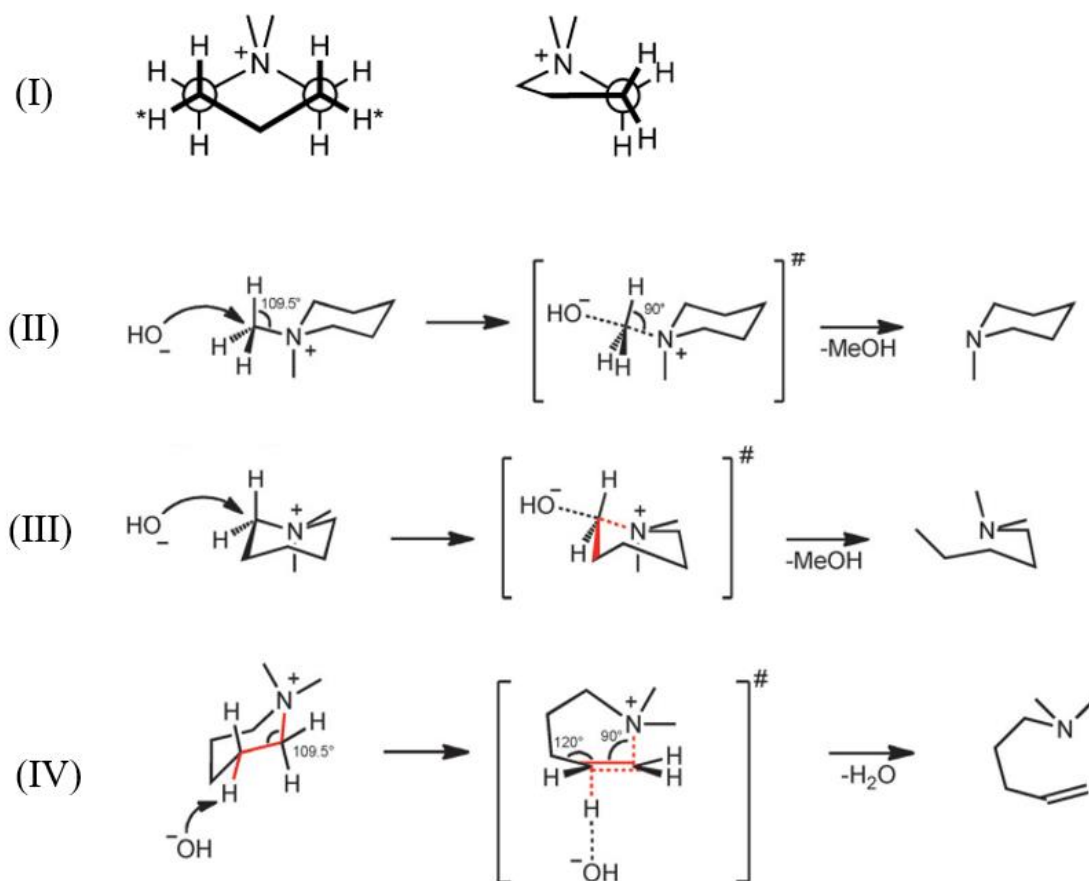


Figure 2.12 (I) Newman projection of MPip and MPyr where β -hydrogens are marked with an asterisk; nucleophilic substitution (II), ring-opening substitution (III) and ring-opening elimination (IV) mechanisms are respectively described.³⁶

2.2 Free Volume Theory

To understand the mechanism underlying the separation of gases with membranes, it is necessary to know the free volume theory. This property is very sensitive to the chemical structure^{102,104} of the polymer determines its viscosity and mechanical properties,⁸⁸⁻⁹⁰ as well as the rates of gas permeability⁸¹ and diffusion. Free volume theory is an extension of two previously developed theories: lubricity⁸²⁻⁸⁵ and gel theory of plasticization.^{85,86}

Free volume is defined as the accessible (empty) space that is inside a polymeric matrix. It is directly related to the glass transition temperature of a polymer (T_g). This means that all the mechanisms that raise the T_g in the same way increase the free volume amount, such as introduce side chains and increase the length of the side chains.⁸⁷ The insertion of an alkyl chain, as in our case using BID monomer, causes an increase in the free movement of the polymer molecules. Modification of the polymer molecules results in a plasticization process, as postulated by Fox and Flory.^{92,93} The importance of the glass transition temperature derives

directly from the fact that below this point the polymer chains are frozen; without the possibility of movement the free volume is significantly lower. Once this limit is exceeded, the polymer becomes free to rotate and move, increasing the unoccupied space.

The arrangement of the free volume is not uniform, but follows a distribution that depends on the thermal energy and its fluctuations. At first, it was assumed that a molecule had to reach a certain activation energy to fill the free volume.⁹⁵⁻⁹⁷ Cohen and Turnbull's model⁹⁴ shed more light on the phenomenon. Assuming a spherical geometry, the molecules could perform the necessary translational motion without any need for energy, if the thermal fluctuation had made available enough free volume for the molecule. We can express this quantity (V_f) as the difference between the volume occupied by the polymer at a given T (V) and the incompressible molecular volume occupied at the thermodynamic zero T (V_0).

$$V_f(T) = V(T) - V_0(T)$$

Given these premises, we can assume V_f as constant below the T_g , while if we consider a higher temperature range, we can use the relation:

$$V_f = V_g + (\alpha_l - \alpha_g)(T - T_g)$$

where V_g is the volume below T_g , α_l and α_g are the thermal expansion coefficient of free volume for the liquid and glass state respectively. For a graphic understanding, we can observe the information already described in **Figure 2.13**.

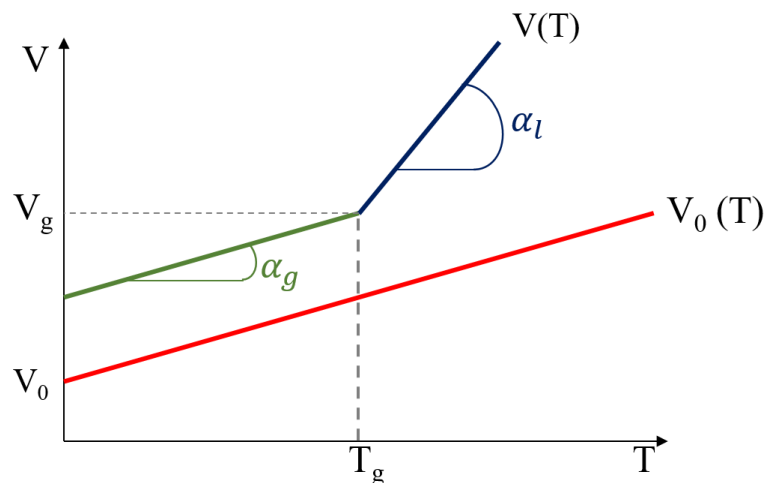


Figure 2.13 Dependence of the volume of a polymer sample based on the temperature at which it is.

2.3 Gas separation

Research focuses on the optimization of membranes to make them competitive with the more used separation methods.^{73,74} We can outline what happens in a system where two gases are separated by a polymeric film by defining the relationship:⁷⁵⁻⁷⁹

$$P = D * S$$

It is useful to note that P (permeability) is the result of two contributions, a kinetic term D (diffusion coefficient), and a thermodynamic term S (solubility coefficient) that determines the driving force within the membrane. The selectivity α of a membrane to a gas A compared to another gas B is defined as:⁸⁰

$$\alpha_{AB} = \frac{P_A}{P_B} = \frac{D_A}{D_B} * \frac{S_A}{S_B}$$

The higher the free volume of the membrane, the higher the permeability, but the lower the selectivity. According to the studies, we can write a new coefficient D where appears the free volume (V_f), a parameter V^* which characterizes the size of diffusing molecules, and write an analytical equation for the permeability:⁷³

$$D = D_0 * e^{\left(\frac{-V^*}{V_f}\right)}$$
$$P = P_0 * e^{\left(\frac{-B}{V_f}\right)}$$

The key parameters for gas separation are the permeability and the separation factor. The performance of a membrane is related to an upper bound relationship, demonstrated by Robeson. The log of the selectivity factor versus the log of the higher permeability gas yielded a limit for achieving a high separation (Robeson's upper bound).⁹⁸⁻¹⁰¹ This relationship was shown to be valid for a multitude of gas pairs including O₂/N₂, CO₂/CH₄, H₂/N₂, H₂/CH₄, and H₂/CO₂. An example for O₂/N₂ is shown below (**Figure 2.14**).

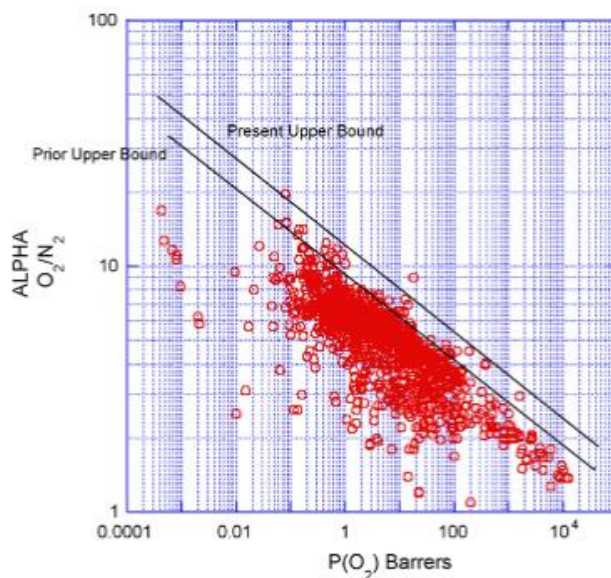


Figure 2.14 Graph of the selectivity against pressure for a gas mixture. The red points are the performance of the polymeric membranes on the market.⁹⁸

2.4 Polymerization and mechanism

Processes of polymerization are divided into two large groups: the first one is the chain-growth polymerization and other one is the step-growth polymerization (SGP). Monomers used for the polymerization are functionalized with different functional groups and can affect the mechanism of the reaction. In fact, if we change the reactivity of these groups it is possible to transform a chain-growth mechanism into a SGP and vice versa.

In a SGP the molecular weight increases slowly at the beginning and very quickly in the end (high conversion). In the usual SGP (Carothers–Flory theory) the molecular weight dispersity (PDI) is around two or even more and the ratio of the monomers A and B is usually 1:1. In the last few years the controlling kinetic factors in SGP have been studied. As a result, it has been discovered a new polymer-forming reactions called condensative chain polymerization (CCP).¹ In this work it will be studied an example of CCP, the superacid *polyhydroxyalkylation*, in all its aspects. A hydroxyalkylation is a Friedel–Crafts reaction; the limitations of this reaction have been well known for a long time like the lower yields and the problematic regioselectivity related to it.

Polyhydroxyalkylation is a reaction between activated and/or non-activated aromatic hydrocarbons with carbonyl compounds in a superacid medium, generally is trifluoromethanesulfonic acid (TFSA). It can be classified as an unusual $A_2 + B_2$ SGP. **Figure 2.15** shows a generic scheme of the reaction.

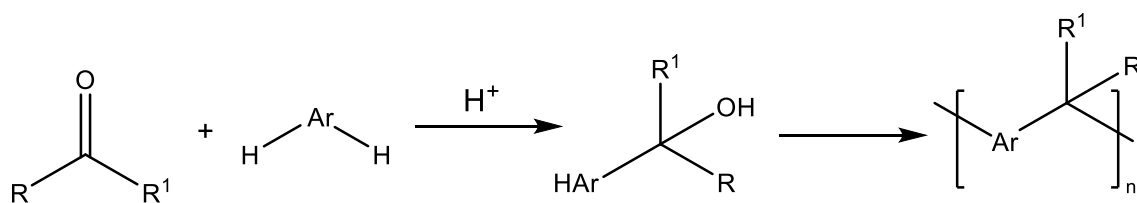


Figure 2.15 Example of a superacid polyhydroxyalkylation.

Furthermore, polyhydroxyalkylation is one-pot reaction; metal-free synthesis; bland and simple conditions like room temperature and atmospheric pressure are required.

One feature observed in the reaction solution is the formation of a “reactive gel”, composed of a polymer that precipitates from the initial homogeneous solution.² Within this precipitate we have two conditions that promote the formation of high molecular weight polymers: a high local monomer concentration and the suppression of cyclization reactions.¹

The last phenomenon to take in consideration is what is called “nonstoichiometric effect”. This effect occurs when the carbonyl compound is in excess of the nucleophile compound.¹ With this condition, it has been observed: decrease in reaction time; allowed to use less reactive monomers; increase in MW; decrease of macrocycles side reactions.^{23,24} This effect is a consequence of the difference in reactivity between the initial carbonyl compound, considered low, and that of the carbinol intermediate which is formed in the first step of the reaction.

For a better understanding of the results, we have to look at the mechanism of the reaction. Since the investigated polyhydroxyalkylation involves isatin and an activated aromatic compound. **Figure 2.16** shows the mechanism between the monomers used.²² In the literature it was described and the following explanation is a summary. The kinetic constant k_1 describes the first step of the reaction where isatin (a), in a superacid media (b), reacts with the nucleophilic monomer (c) to lead a carbinol intermediate. At this point, it has different paths to follow. If it reacts with another molecule of (c) the product is the dimer (f) and constant k_2 ; otherwise it could react with another carbonyl compound to lead a dicarbinol specie (g) with a k_3 constant; last option is the product (h) and k_4 . To investigate the right path some assumptions were made: kinetic rate constant k_3 is very small compared with the others because of the high energy of activation that is required to lead the dicarbinol compound; the speed rate of k_2 is the same or faster than k_3 ; monomers (a) and (c) reacts faster than (e) with (e). In general it is obtained $k_1 > k_4 > k_2 \geq k_3$. Under this conditions the favored product is (h). The reaction that involve two (h) chain is slower allowing a fast increase in M_n and limiting the increase of the

polydispersity. Since the reaction between (h) and (g) is the slowest, an excess of carbonyl compound will increase the molecular weight.

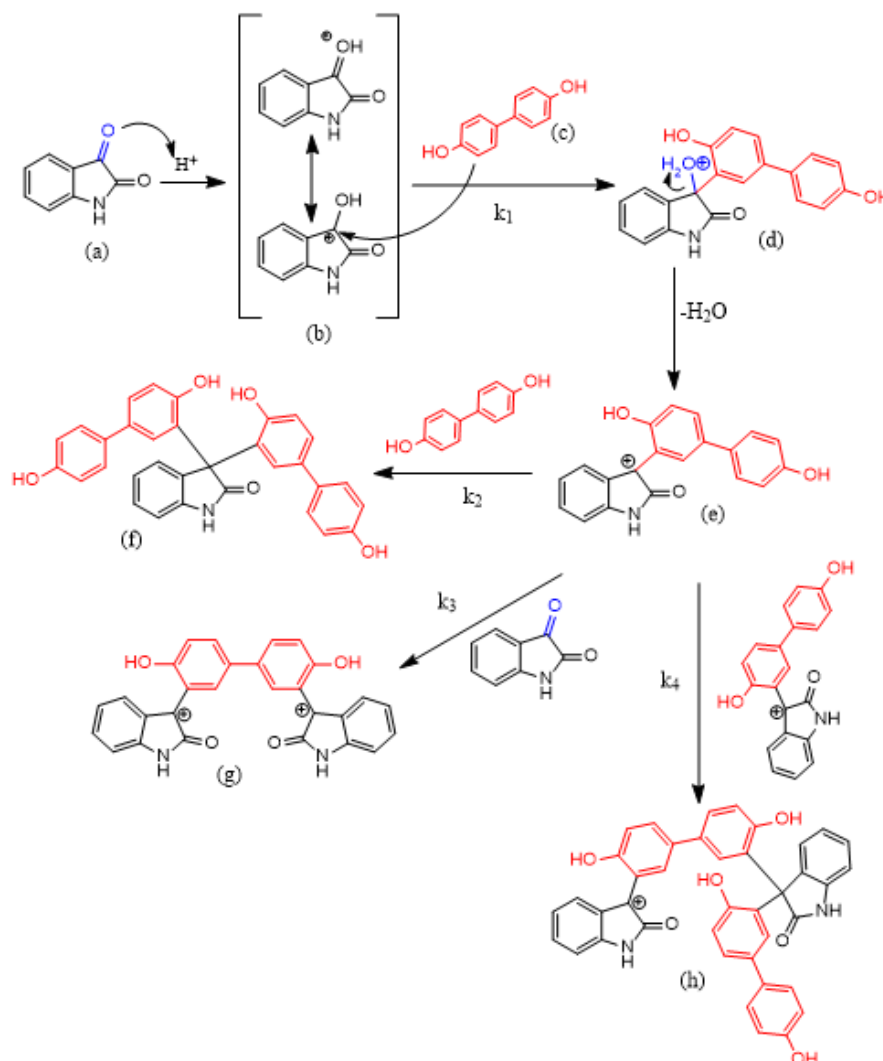


Figure 2.16 Mechanism scheme for superacid polyhydroxyalkylation of isatin and 4,4'-dihydroxybiphenyl.²²

This mechanism implies a decrease in nucleophilicity with the increase of the chains length. It is therefore necessary to consider that what occurs is a protonation of the indole fragment. This creates a net positive charge, reducing the reactivity of the entire chain, as shown in **Figure 2.17**. This phenomenon is crucial for obtaining a narrow polydispersity. If this were not the case, a classic SGP with PDI greater than 2 would be obtained.

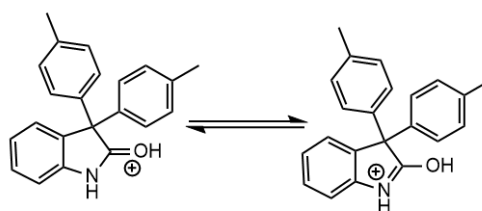


Figure 2.17 Protonation of the oligomers.

In theory, it would be legitimate to think that a superelectrophilic system is formed in this reaction environment.¹¹⁰ Basically, it was investigated whether the really reactive species was the electrophile in the form of cation or dicationic. In the literature, quantum mechanical calculations were carried out on the system is shown in **Figure 2.18**. Isatin has three acidic sites. Furthermore, we know that the reaction must go through the reaction intermediate that has the protonated carbonyl ketone (c). The reaction complex that isatin forms with the electrophile is the determining step of the reaction (e),(f). To estimate the relative contribution of mono- and diprotonated intermediates to the reaction mechanism, one should compare the Free Gibbs energy of diprotonated species with the total one calculated for monoprotonated isatin and the corresponding energies of second protonation.¹⁰⁹

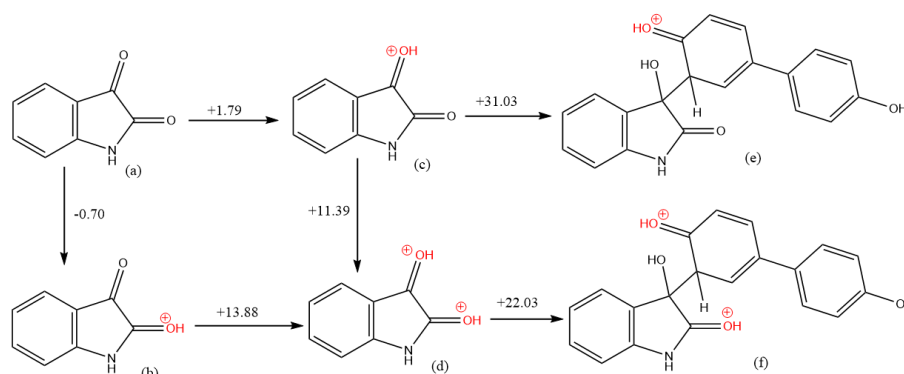


Figure 2.18 isatin (a); amide carbonyl protonation (b); ketone carbonyl protonation; dicationic specie (d); monocationic complex (e); dicationic complex (f).

From the results of the calculations it is observed a $\Delta_{c \rightarrow e} = 31.03$ (kcal/mol), while $\Delta_{c \rightarrow d \rightarrow f} = 33.42$ (kcal/mol). It can be assumed that, in the mechanism of the reaction, the monocationic species is the reactive one.

2.5 Characterization methods

2.5.1 Size exclusion chromatography (SEC)

SEC is a fundamental characterization technique with which molecules can be separated based on their size through gel filtration,¹¹⁵ first discovered by Synge and Tiselius.¹¹³ The gel phase

is formed by a porous matrix of a certain size distribution. The separation occurs as the smaller molecules enter the porosities, and their flow in the column is slower. Conversely, the larger molecules do not interact with the pores and take less time to travel down the column, as shown in **Figure 2.19**.

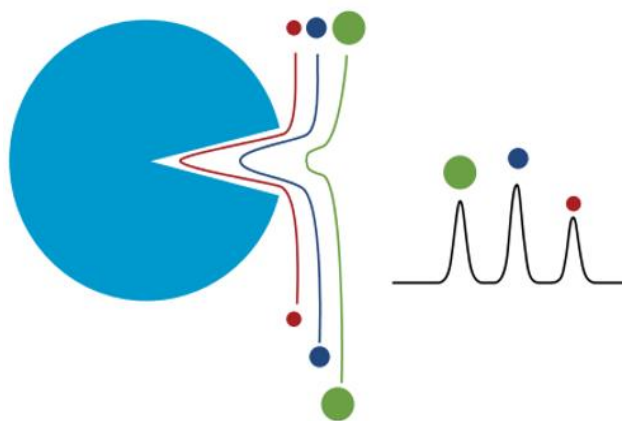


Figure 2.19 Interaction of molecules with the stationary phase based on size. ¹¹²

SEC performs two types of separations: fractionation and desalting. Each chromatographic column is built to certain specifications, which determine its resolution. In the case of fractionation, each column is set up to effectively separate molecules in a given MW range. The specific factors involved are particle size, pore size, flow rate, column length and diameter, and sample volume. The smaller the particle size, the higher the final resolution. Pore size controls the exclusion limit and the fractionation range of the media. The optimal flow-rate depends directly on the media used. A moderate flow allows small molecules to fully access the pores present in the stationary phase. This increases the MW partition. Too slow flow-rate leads to elongation of the bands due to too slow diffusion. A longer and larger diameter column leads to increased resolution and greater volume capacity. Void volume (V_0) at the top of the column can significantly reduce resolution as the sample is allowed to diffuse prior to entering the column bed. In addition, you have to make sure that the packing of the column is right. An overpacked column can collapse the pores in the stationary phase resulting in diminished resolution. On the other hand, an underpacked column increases the mixing volume outside of the pores, resulting in broader, less resolved, peaks.

The final result of a SEC analysis is called chromatogram and an example is illustrated in **Figure 2.20**. We can see how high MW polymer are eluted very fast due to no interactions with the stationary phase, unlike the low MW. Salts and solvent are not separated and are eluted at the total liquid volume (V_t). We can define a retention volume for each molecule (V_r).¹¹⁴

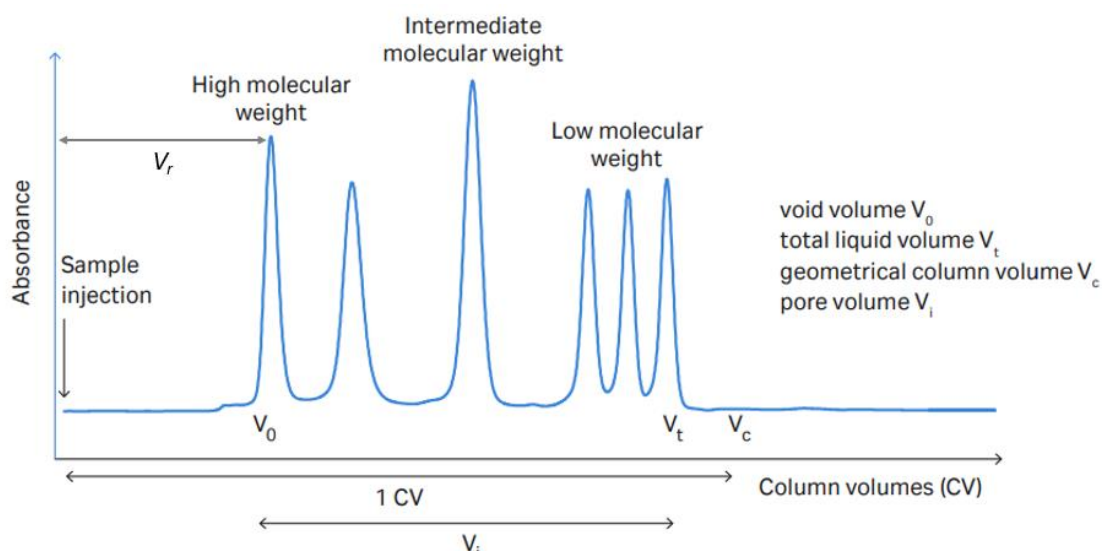


Figure 2.20 Example of chromatogram with all factors.¹¹⁴

To compare these results between different columns and to describe more accurately the behaviour of the molecules, a partition coefficient k_d is defined. It describes how a molecule is distributed between stationary phase and mobile phase. The relation to define the constant is:

$$K_d = \frac{V_r - V_0}{V_t - V_0}$$

Large molecules will have a K_d equal to 0 whereas small molecules will have a K_d equal to 1. More technically, the column separates polymers based on their hydrodynamic volume, which is directly proportional to the molecular weight and intrinsic viscosity ($V_H \propto MW[\mu]$).

By exploiting this relationship, it is possible to identify a relationship that binds the molecular weight to the retention volume:

$$\log MW = \log A - BV_r$$

where A and B are constants related to the interaction between polymer and solvent used.

Other important indicators can be obtained, such as the numerical average molecular mass (M_n) and the weight average molecular mass (M_w), and from the relationship between these the polydispersity index (PDI).

Samples for size exclusion chromatography were prepared by dissolving 1 mg of polymer per mL of solvent (THF) for at least one day. Then, samples were filtered twice through a Teflon syringe filter (Millex LS, 0.2 μm).

2.5.2 Thermal gravimetric analysis (TGA)

Thermogravimetry is an analysis method that allows to study the thermal stability of the materials. The technique consists in evaluating the percentage variations in weight of a sample under at rising temperatures. The sample is placed on a crucible, which can be Pt or alumina depending on the desired maximum temperature to reach. The crucible is then placed inside a furnace and is subjected to a programmed temperature in a predetermined atmosphere (commonly air or nitrogen). Weight variations associated with temperature increases are then recorded. It is possible to pair a second analysis tool, such as GC or FTIR, to the instrument that performs TGA in order to analyse the degradation products of the tested substance. In the field of polymer science, this technique is widely used as it allows to study the thermal degradation of the polymer and product composition. In particular, from the thermogram it is possible to obtain the polymer degradation temperature.

Thermogravimetric analysis (TGA) was provided using a TA Instruments Q500 Analyzer in N₂ atmosphere. The procedure includes:

1. Equilibration at 110 °C to remove water content;
2. Isothermal for 10 min;
3. Equilibration at 50 °C;
4. Heating from 50 °C to 600 °C at a heating rate of 10 °C min⁻¹.

2.5.3 Differential scanning calorimetry (DSC)

Differential scanning calorimetry (DSC) is a technique used to investigate the response of polymers to heating process. The instrument is formed by a measurement chamber and a computer. Two pans are heated in the measurement chamber, which one contains the sample and the second is used as a reference. The computer is used to monitor the temperature and regulate the rate at which the temperature of the pans changes. Physical and chemical changes create a temperature difference between the two pans. The thermogram shows the trend of the thermal flow, in which these differences are highlighted. DSC can be used to study the melting (T_m) and crystallization (T_c) temperature or the glass transition (T_g). In **Figure 2.21** is shown a typical thermogram in which all transitions are investigated. All samples were analysed in two heating cycles to remove any thermal history using a Q2000 DSC (TA Instruments) at 10°C min⁻¹ heat flow rate.

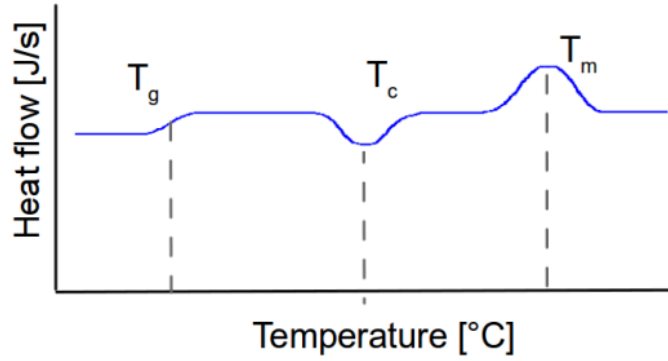


Figure 2.21 Thermogram with glass (T_g), melting (T_m) and crystallization (T_c) transition.

2.5.4 Water uptake

The water uptake (WU) of the samples is determined by comparing the weight of the dry membranes (W_{OH}) and that of those left in an aqueous solution for several days (W'_{OH}).

$$WU(\%) = \frac{W'_{OH} - W_{OH}}{W_{OH}} * 100\%$$

However, due to issues with the membrane degradation in OH^- form, the dry weight is calculated from W_{Br} using the titrated IEC. Assuming quantitative conversion in ion exchange from bromide to hydroxide we can associate W_{Br} with W_{OH} as:

$$W_{OH} = W_{Br} - \frac{W_{Br} * IEC_{Br} (MM_{Br^-} - MM_{OH^-})}{1000}$$

2.5.5 Ion exchange capacity (IEC)

The value of the IEC represents the number of functional groups per unit mass of the polymer. The determination of this parameter is not carried out directly through an acid-base titration as the membrane is exposed to alkaline degradation due to the OH^- and, moreover, it is possible that a reaction occurs between the counter ions present in the solution and the CO_2 that is solubilized. These factors make the result less accurate. The IEC_{OH} value is indirectly measured using the IEC_{Br} , determined by Mohr titration. The membrane in its bromide form is weighed and dried. It is then immersed in a sodium nitrate solution ($NaNO_3$) of known molarity for several days to allow the exchange of all the bromine groups. The final solution is titrated with silver nitrate ($AgNO_3$) and the relationship below is used to determine the quantities of interest.

$$IEC_{OH} = \frac{IEC_{Br}}{1 - \frac{IEC_{Br}(MM_{Br^-} - MM_{OH^-})}{1000}}$$

2.5.6 Hydroxide Conductivity

The hydroxide conductivity is measured by electrochemical impedance spectroscopy (EIS).¹⁶⁰ In this analysis a sinusoidal potential [E], with an amplitude [E₀] and with frequency [ν] values between 10⁰ and 10⁷ Hz, is applied to a sample during a certain time [t]. The results in an alternating current [I] with amplitude [I₀] that is shifted with a [φ] phase angle (**Figure 2.22**).¹⁷²

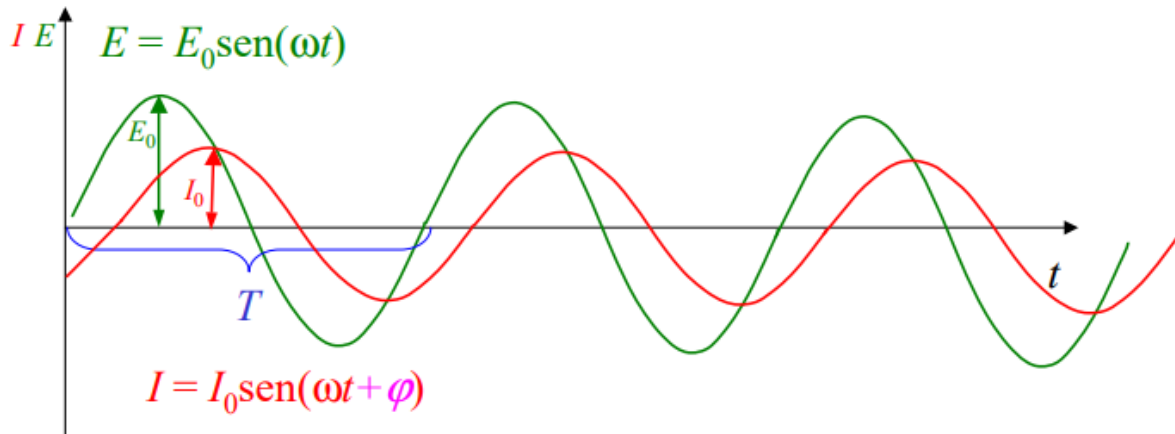


Figure 2.22 The time dependence of the alternating current applied.¹⁶³

The instrument measures impedance Z as a function of frequency. It is defined as the length of the vector |Z| and the phase angle φ (**Figure 2.23**). As we can see from the mathematical relationship¹⁶⁴ that links the impedance to its graphic description, Z is a complex quantity and can be divided into a real part Z' and an imaginary part Z''.¹⁶⁵

$$|Z| = \frac{E_0}{I_0} = \sqrt{Z'^2 + Z''^2}$$

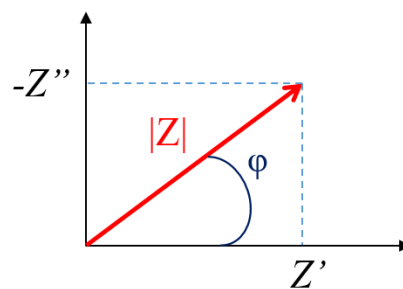


Figure 2.23 Graphic visualization of impedance.

The membrane is placed between two electrodes. The system is completely immersed in a solution to avoid contact with CO₂. By plotting the two components of Z we can construct what is called a Cole-Cole graphic¹⁶⁸⁻¹⁷¹ and an ideal example is shown in **Figure 2.24**. From these results we can highlight the following information: the semicircle is the membrane performance

while the slope is the electrode ones. The identified point separating the two curves, which corresponds to the diameter of the semicircle, is defined as membrane resistance R_b .

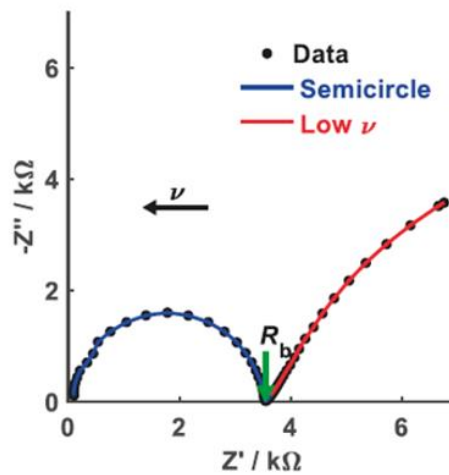


Figure 2.24 Cole-Cole plot.

Ionic conductivity σ can be calculated using the relationship¹⁶⁶⁻¹⁶⁷

$$\sigma = \frac{d}{A * R_b}$$

where d is the distance between the electrodes and A is the cross-sectional area through which the ions are transported.

2.5.7 Alkaline stability

To determine the alkaline stability, pieces of the membranes are immersed at a high temperature (90 – 120 °C) in a solution typically of KOH or NaOH. At selected intervals the samples are extracted, the bromide ions are restored in order to carry out an NMR analysis. From the results it is possible to determine the degree of degradation of the quaternary cations, the type of decomposition products that are obtained and understand which is the dominant degradation mechanism.

3 Experimental methods

This chapter is divided into two parts. The first is focused on the synthesis methodologies of the monomer necessary for polymerization, and of the two polymers studied. The second part is aimed to the synthesis of functionalized polymers and the preparation of membranes. NMR spectroscopy was used to study and verify the molecular structures of synthesized monomers and polymers. On a Bruker DRX400 spectrometer, ^1H and ^{13}C NMR spectra were obtained at 400 and 100 MHz, respectively. Solvents used for the analysis include DMSO- d_6 ($\delta = 2.50$ ppm).

3.1 Monomer synthesis

In literature there are some procedures for the synthesis of BID (**Figure 3.1**),¹⁰⁷ but the most challenging part turns out to be the purification of the compound. Five grams of isatin was dissolved in 33 mL DMF (12 eq). Subsequently, 9.4 g of potassium carbonate (2 eq) and 16.3 mL 1,4-dibromobutane (4 eq) were added to a 500 mL flask. While stirring the system, the isatin solution was dropped into the flask. To accelerate the reaction, the temperature was raised to 60 °C.

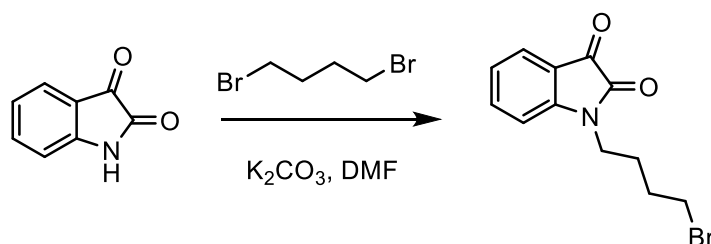


Figure 3.1 Synthetic scheme of BID.

The reaction was monitored by TLC as shown in **Figure 3.2 (a)**. After all the isatin reacted, the TLC revealed a by-product due to a side reaction.

The amide compound is the limiting reagent and it is highly diluted in the solvent to avoid unwanted reactions. The final solution was filtered to remove the residues of K_2CO_3 , while the excess of 1,4-dibromobutane was distilled off under reduced pressure at 140 °C. The solution was purified through a solvent extraction (ethyl acetate / water) two times to remove aqueous soluble by-products and DMF. The organic layers were collected and analysed by NMR, showing presence of impurities. A vacuum silica gel chromatography column was used to isolate the product from the impurities. The eluent used was heptane / ethyl acetate 4:1. The dark red solution containing the product was concentrated by rotavapor and recrystallized with

ethanol as solvent. The final product was an intense dark red needle crystal (**Figure 3.2 (b)**). The yield was 65%.

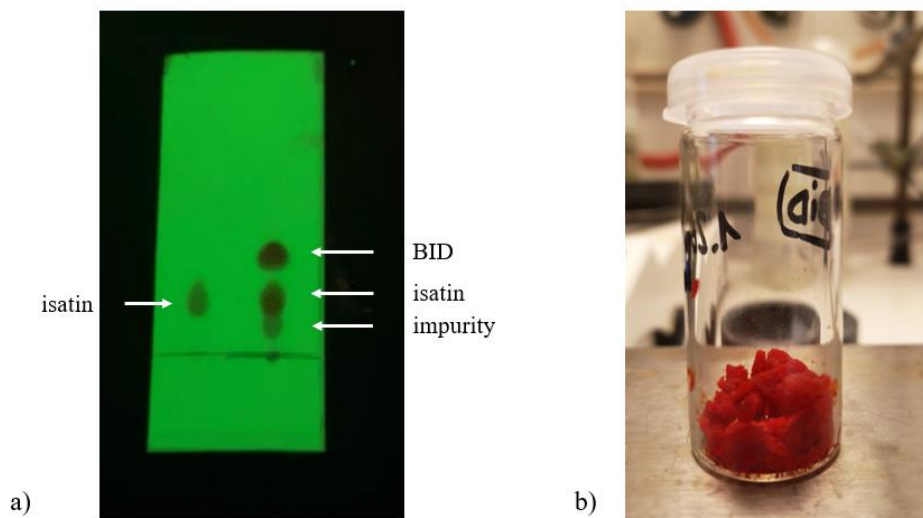


Figure 3.2 TLC to monitor the reaction progress (a) and crystals of BID (b).

After the purification process, the NMR sample was prepared by dissolving 0.010 g of product in DMSO- d_6 .

3.2 Synthesis of PSIX

Figure 3.3 shows the synthetic route of the polymer; isatin (A) and 4,4'-Dihydroxybiphenyl (B) are the monomers used.

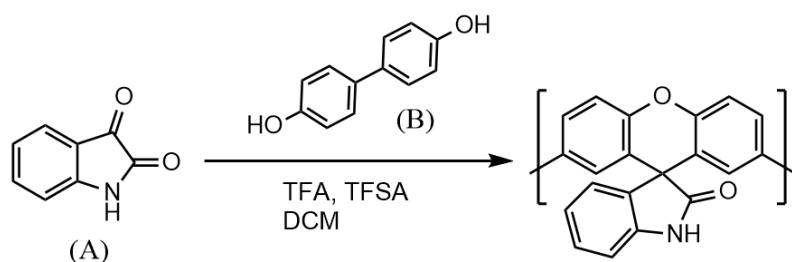


Figure 3.3 Reaction scheme to obtain PSIX.

Monomers A and B were added to a 10 mL flask with TFA (and DCM where necessary). At this point, the TFSA was slowly added keeping the system immersed in an ice bath. The flask was then sealed. Solution changed from orange to black very quickly, then turned dark brown over a variable period of time. The solution subsequently had turned dark green and had increased viscosity over time.

Work-up:

All reactions were stopped by gently pouring the viscous solution into methanol, precipitating the polymer as a white fibrous solid. The solid obtained was filtered and resolubilized in NMP or DMSO. At this point we can see the amount of gel formed during the polymerization. After reprecipitating the polymer into methanol and filtering it, the solid was dried under vacuum at 50 °C.

3.3 Synthesis of PBSIX

The synthesis of poly (1- (4-bromobutyl)-2',7'-spiro [indoline-3,9'-xanthen]-2-one), denoted as PBSIX, was very similar to that of the previous polymer, as shown in **Figure 3.4**.

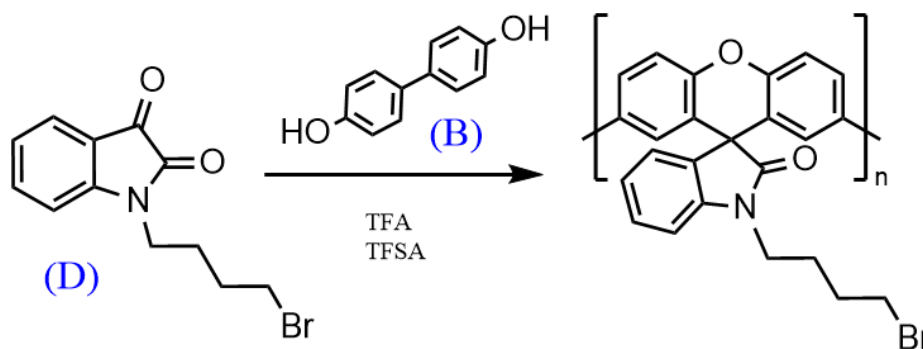


Figure 3.4 Synthesis of PBSIX.

Monomer D (BID) and B were added to a 10 mL flask with TFA and then TFSA was added. An optimization of the reaction was not carried out, but the most favourable conditions found from the previous synthesis were taken as starting ones. The reaction conditions used are shown in **Table 1**.

Table 1 Reaction conditions of PBSIX synthesis.

ENTRY	BID(g)	BIPHENOL(g)	TFA(mL)	TFSA(mL)	RT (h)	D:B	TFSA:D
D1	0.148	0.093	0.5	0.5	26	1.05	11
D2	0.317	0.205	0.9	0.9	uf	1.02	9
D3	0.148	0.093	0.4	0.4	31	1.05	8.5
D4	1.633	1.026	5.5	5.5	79	1.05	10.8
D5	1.501	0.9405	5.1	5.1	47	1.05	10.8

The next step was to scale up the reaction to obtain larger quantities of product. To make the measurements comparable with each other, the polymer should be provided from the same batch for all the membranes.

The work up of the reaction was the same as previously described. The polymer solution was precipitated in methanol and the solid filtered. The polymer was solubilized in DMSO (5 wt%), obtaining a honey-coloured viscous solution. In this case, there was no evidence of gel formation. Once re-precipitated in methanol, the product in the form of powder was left in the oven (50 °C) to dry under vacuum.

3.4 Polymer modification and functionalization

The functionalization procedure was quite similar in the three cases studied. A polymer sample was weighed and a 5 wt% solution in a suitable solvent was prepared. After a homogeneous solution had been obtained, 10 equivalents of the amine solution were added. The trimethylamine used was a 45 wt% solution in water, while the others were pure. **Figure 3.5** shows the synthesis pathways.

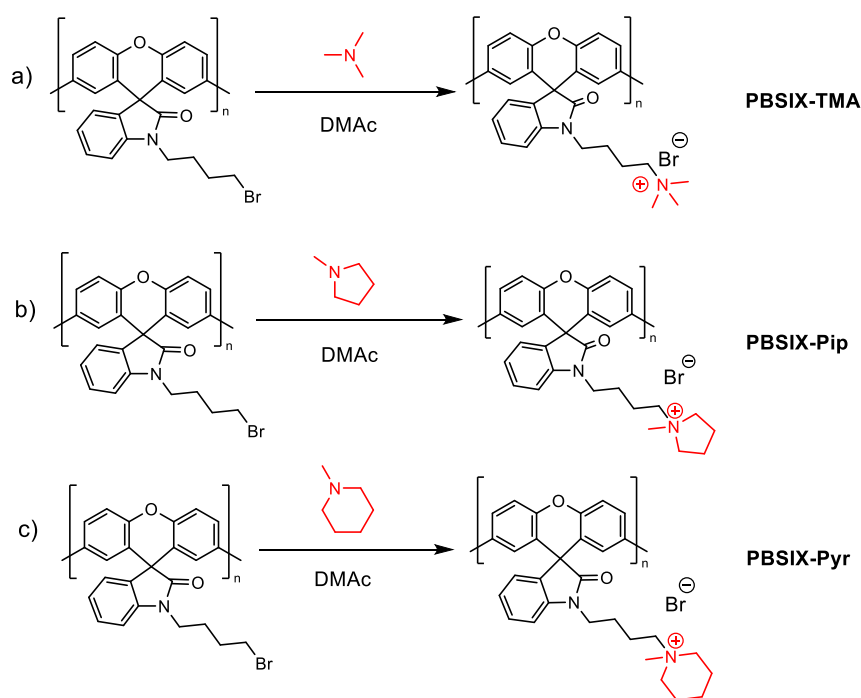


Figure 3.5 Quaternization reactions of the polymer with different types of amines to obtain the polymer functionalized with a QA.

The reaction conditions were not the same for all. To obtain PBSIX-TMA (**a**) it was sufficient to leave the reaction for less than a day at room temperature. The reaction between the polymer

and *N*-methylpyrrolidine **(b)** and *N*-methylpiperidine **(c)** to obtain respectively PBSIX-Pyr and PBSIX-Pip was much slower and took 7 days at 85 °C.¹⁶²

3.5 Membrane preparation

All films included in this thesis were prepared by solvent casting (**Figure 3.6**) from 5 wt% or 10 wt% polymer solutions placed in Petri dishes ($\varnothing = 5$ cm). The solutions, prepared with DMSO or NMP, were filtered using a Teflon syringe filter (Millex LS, 5 μm) and left in a casting oven at 80 °C or in the fume hood for 24 h.

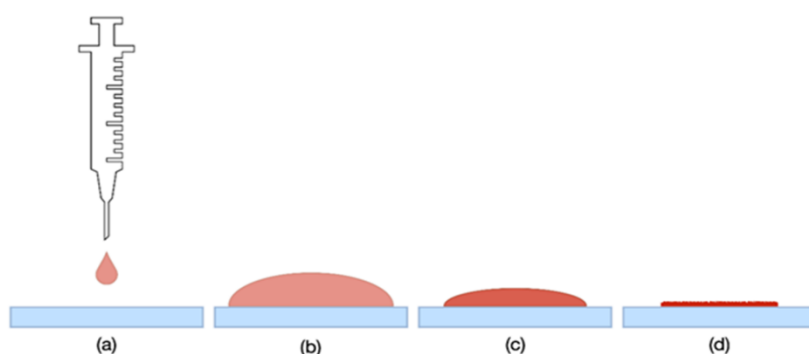


Figure 3.6 Process of film forming with the casting technique.

4 Results and Discussion

4.1 Monomer characterizations

4.1.1 Isatin

During the first steps, the work was based on the use of the isatin [indoline-2,3-dione], whose structure is shown in **Figure 4.1**. Isatin, obtained for the first time in 1841, is a molecule that has shown increasing importance over the years. Thanks to its synthetic versatility and its availability, it is fundamental in the modern synthesis of many organic compounds.¹⁰⁵

According to the literature,^{105,173} the ¹H NMR spectrum (**Figure 4.1**) of isatin showed the signals of the aromatic nucleus H-7 and H-4 at $\delta = 6.92$ and 7.51 as doublets. At $\delta = 7.07$ and 7.59 triplets were observed corresponding to H-5 and H-6, respectively. The hydrogen atom (H-1) attached to nitrogen appeared as a singlet at approximately 11.03 ppm in DMSO-*d*₆.

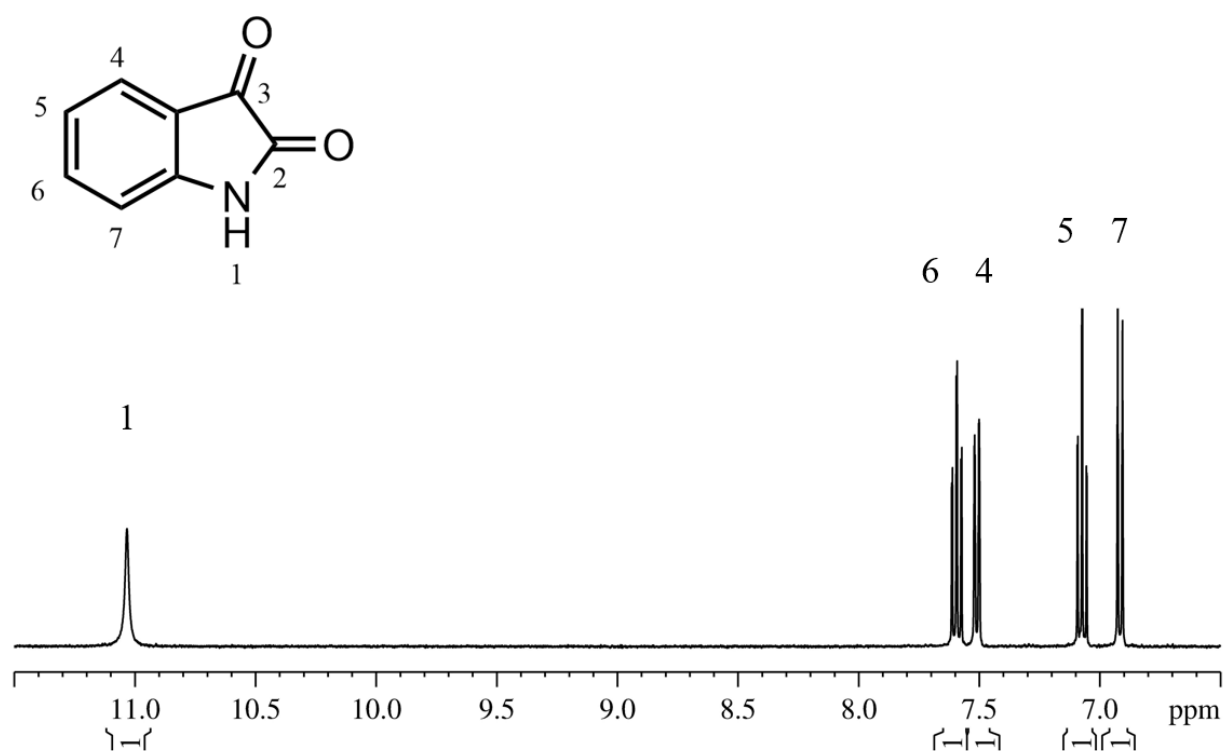


Figure 4.1 ¹H NMR spectrum of isatin in DMSO-*d*₆.

The first time isatin was characterized, the assignment of the chemical shifts of the isatin carbons (**Figure 4.2**) has instead been the subject of controversy. The correct assignment was

then confirmed as follows:^{105,3} δ 184.9 (C-3), 159.8 (C-2), 151.2 (C-7a), 138.8 (C-6), 125.2 (C-4), 123.2 (C-5), 118.3 (C-3a), 112.7 (C-7).

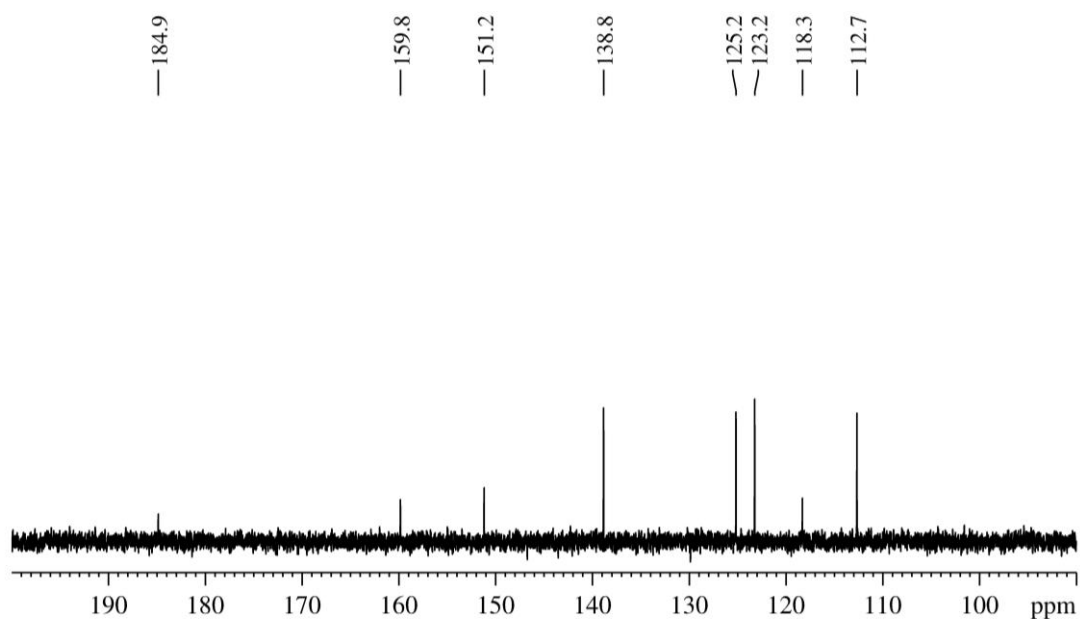


Figure 4.2 ¹³C NMR spectra of isatin in DMSO-d₆.

4.1.2 BID

In order to maximize the yield, the reaction was carried out changing certain factors. We tried the synthesis at room temperature and at high temperature as well. At 25 °C the reaction was too slow, in fact after 12 hours of reaction time and purification process the yield was below 25%. Another way to perform the reaction was using acetonitrile as solvent instead of DMF. Unfortunately the solubility of isatin in the solvent was low and the mixing process inside the flask between reagents was visible difficult. The most challenging part during the purification was to obtain BID as a solid. This was related to the extreme sensitivity to impurities of BID.

The by-products resulting from BID synthesis were of two types. One was characterized by water solubility and different aromatic chemical shifts compared to the BID ones. The second by-product showed different chemical shift in the aliphatic region compared with BID spectrum. **Figure 4.3** shows the consecutive reactions that lead to the formation of the hypothesized by-products. Reaction (a) shows the double N-addition to give the quaternary ammonium salt. Reaction (b), on the other hand, shows a cross-linking reaction where both bromine atoms reacted.

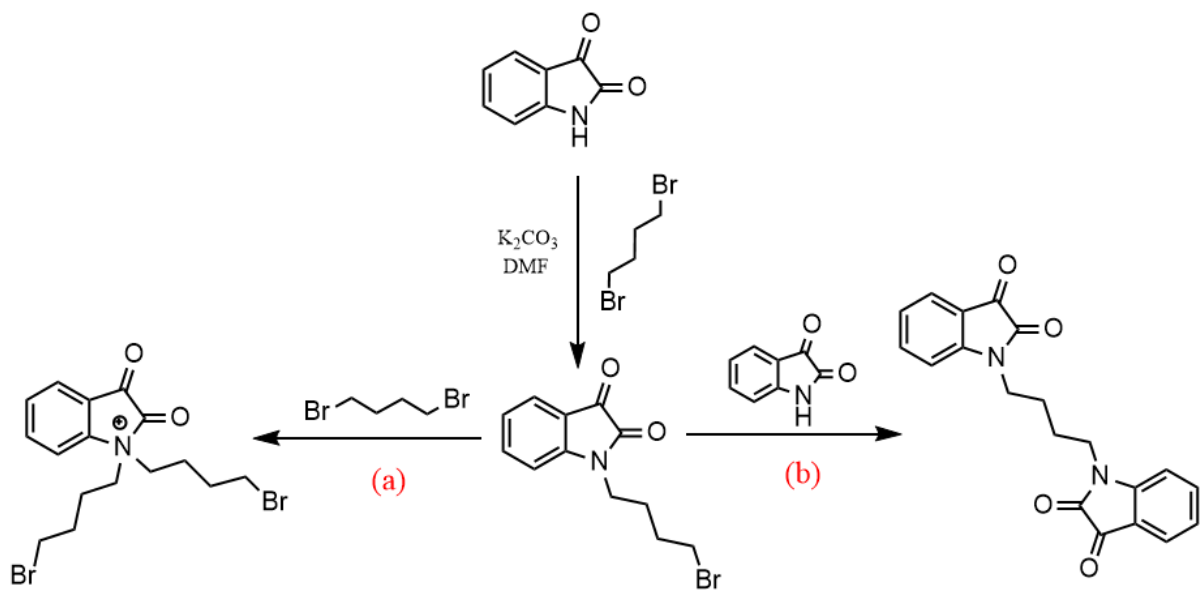


Figure 4.3 Side reactions of BID that lead to by-products.

The NMR spectrum was shown in **Figure 4.4**.¹⁰⁷ We expect a certain degree of analogy between the aromatic region of BID and isatin. The insertion of an alkyl chain and a bromine atom has a deshielding effect on the protons, which resonate at a higher frequency. The assignments are the following: H₃ at δ 7.67 (t), H₁ 7.55 (d), H₄ 7.21 (d) and H₂ 7.14 (t). The proton with the highest chemical shift compared to isatin is H₄. This is due to the proximity to the substituent group.

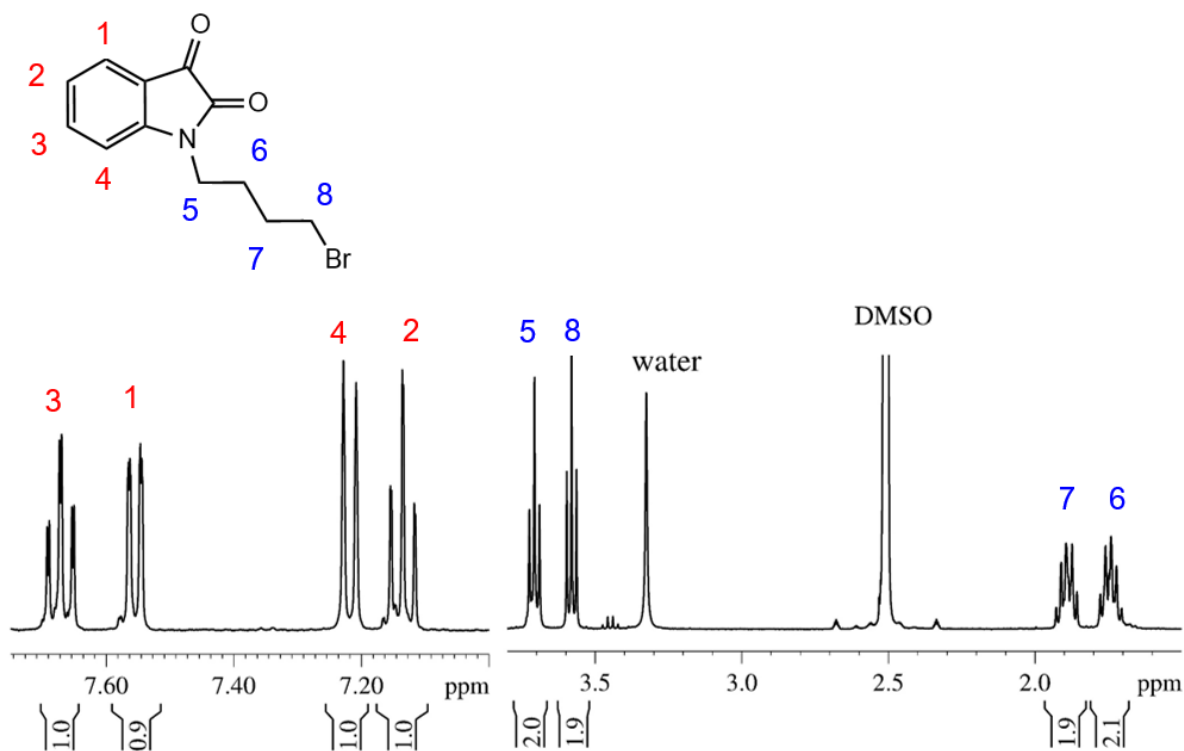


Figure 4.4 ^1H NMR spectra of BID in $\text{DMSO-}d_6$.

The aliphatic chain should be visible as two triplets for the terminals $-\text{CH}_2$ and two quintuplets for the $-\text{CH}_2$ in the middle. We can see confirmation, defining 5- CH_2 at δ 3.71 (t) and 8- CH_2 at 3.58 (t). The remaining 7- CH_2 and 6- CH_2 were found at δ = 1.9 and 1.7, respectively.

It is interesting to evaluate the impact of the substituent also on the chemical shifts of the carbons, as shown in **Figure 4.5**.

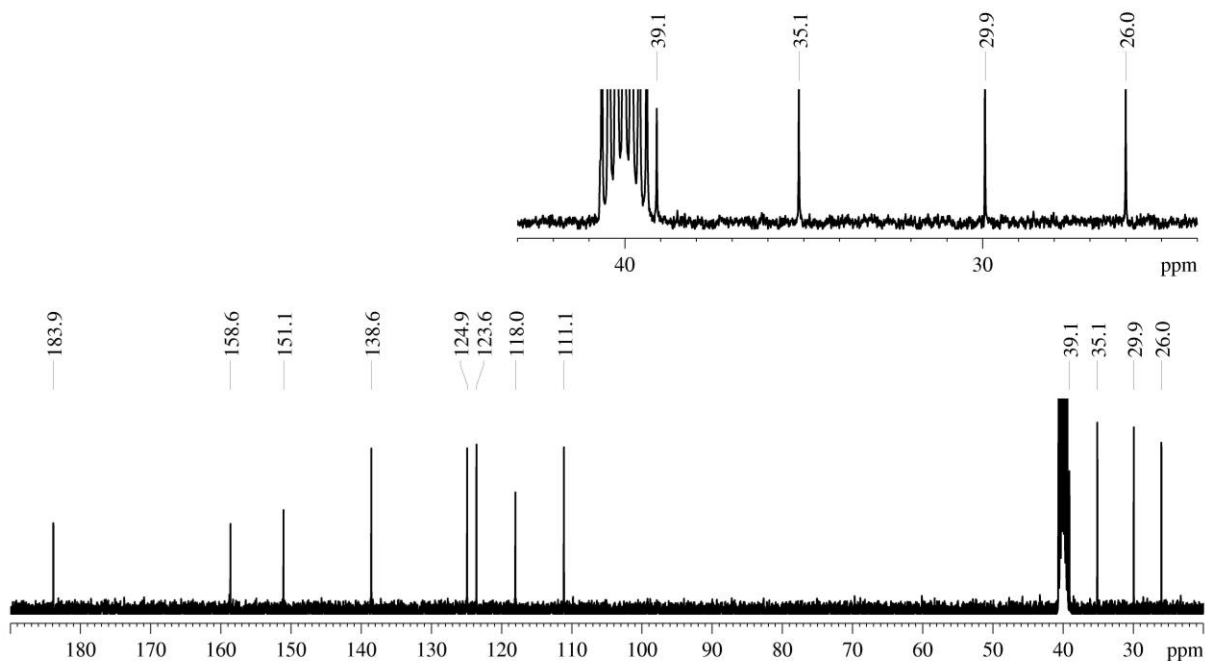


Figure 4.5 ^{13}C NMR spectra of BID in in $\text{DMSO-}d_6$.

The experimental data did not show a relevant effect in ^{13}C chemical shift. The assignment made for isatin is also valid for BID. The carbons with the highest chemical shift are the ketone carbonyl (δ 183.9), which is more unshielded, and the amide carbonyl (δ 158.6), respectively. Chemical shift at δ 151.1 and 118.0 are the quaternary C. The assignments of aliphatic carbons were not investigated.

4.2 Polymer characterizations

4.2.1 PSIX

In this project, the aim was to obtain a membrane of PSIX. Therefore, high molecular weight of the polymer is required for film-forming properties. For this reason, an optimization of the polymerization was necessary.

PSIX was synthesized by superacid hydroxyalkylation. This reaction can take place only in super acid media,^{25,26} where pK_a of the solution is less or equal to -11.5. The value of the pK_a of TFA is 0.52,¹⁶ that of the TFSA instead is -14.7 (± 2).¹⁰⁸ Two reaction mediums were tested: TFSA in TFA as solvent and a mixture of TFSA and TFA in anhydrous DCM as solvent. The three crucial factors involved in determining to yield linear high-molecular-weight polymer²⁷ were: TFSA/carbonyl ratio; A_2/B_2 ratio; diffusion constant.

An increase in TFSA should lead to an increase in molecular weight. Further increase in the proportion of TFSA resulted in possible cross-linking. Another aspect to consider was the

reactivity of the monomers. In fact, polymerizations with weak nucleophiles required a stronger medium or an increase in proportion of TFSA, meanwhile with biphenols the system was enough reactive.³

The challenge was to reach high conversion and high MW without forming cross-linked chains and gel particles. The reaction time was effected by the ratio of TFSA, of monomers and the stirring rate of the reaction mixture . The optimization of the polymerization started with a 1 : 1 ratio between the monomers and continued with an increase in the amount of carbonyl compound to investigate the change in polymer MW and speed of the reaction. The control of the reaction time is one of the most essential factor to try to reduce the gel formation. The aim was to increase the reaction time enough to obtain a high MW with the minimum amount of gel formation.

In the following tables are reported various employ reaction conditions. Data are grouped according to the stoichiometry of the monomers, starting with **Table 2** where all the experiments carried out with a 1 : 1 ratio of isatin and 4,4'-dihydroxybiphenyl are reported.

Table 2 Reactions with equimolar A:B; uf: unfinished; night:

<i>Entry</i>	<i>A(g)</i>	<i>B(g)</i>	<i>TFA(mL)</i>	<i>TFSA(mL)</i>	<i>DCM(mL)</i>	<i>RT (min)</i>	<i>A:B</i>	<i>TFSA:A</i>
A1	0.19	0.240	0.85	1.4	1.2	uf	1.00	12.5
A2	0.22	0.278	0.80	1.5		uf	1.00	11.5
A3	0.22	0.278	0.90	1.3		uf	1.00	10.0
A4	0.35	0.440	0.20	1.9	1.9	2	1.00	9.00
A5	0.22	0.278	1.00	1.0		uf	1.00	7.50
A6	0.24	0.304	0.50	1.0		8	1.00	7.00
A7	0.22	0.278	1.00	0.9		427	1.00	7.00
A8	0.35	0.440	0.20	0.9	1.9	3	1.00	4.30
A9	0.35	0.440	0.20	0.4	1.9	10	1.00	2.00

We can notice that the outcomes follow two opposite trends: reactions took place extremely fast or did not took place at all. It was observed that if TFA and TFSA were added sequentially, the reaction was very fast (entry A4, A6, A8, A9). The reactions were stopped when the viscosity

of the final solution was very high but they resulted in gel formation. There was no way to control the reaction.

Otherwise, if we waited 30 minutes before adding TFSA the reaction took longer time (entry A7), or never started (entry A1, A2, A3, A5); in fact, it was noted that in failed (i.e. unfinished) experiments the solution neither turned from dark brown to dark green, nor did it change in viscosity. The final polymer obtained with these conditions was not film forming.

Table 3 Reactions with A:B= 1.02:1

<i>Entry</i>	<i>A(g)</i>	<i>B(g)</i>	<i>TFA(mL)</i>	<i>TFSA(mL)</i>	<i>DCM(mL)</i>	<i>RT (min)</i>	<i>A:B</i>	<i>TFSA:A</i>
B1	0.22	0.279	0.70	1.2	0	75	1.02	9.0
B2	0.22	0.279	1.00	1.2	0	117	1.02	9.0
B3	0.22	0.279	1.00	1.2	0	102	1.02	9.0
B4	0.22	0.279	1.00	1.2	0	205	1.02	9.0
B5	0.22	0.279	1.00	1.2	0	313	1.02	9.0
B6	0.22	0.279	0.70	1.0	0	20	1.02	7.5
B7	0.22	0.279	0.70	1.0	0	31	1.02	7.5
B8	0.24	0.298	1.00	1.0	3	296	1.02	7.0

Next step was to increase the excess of isatin to 2%. The results were shown in **Table 3**. The increase in isatin ratio resulted in a longer reaction time, as we can see from entry B2, B3, B4, B5 and B8. The polymer obtained with these conditions showed some film forming properties, even if the gel formation was still present. The main issue was the reproducibility of the experiments. Although the conditions were the same, the variability of the results was large.

Table 4 Reactions with A:B= 1.05:1

Entry	A(g)	B(g)	TFA(mL)	TFSA(mL)	DCM(mL)	RT (min)	A:B	TFSA:A
C1	0.23	0.278	0.90	1.6		126	1.05	11.5
C2	0.23	0.278	0.90	1.6		106	1.05	11.5
C3	0.23	0.278	0.90	1.6		80	1.05	11.5
C4	0.23	0.278	0.90	1.6		100	1.05	11.5
C5	0.23	0.278	0.90	1.5		116	1.05	11.0
C6	0.23	0.278	0.90	1.5		108	1.05	11.0
C7	0.23	0.278	0.90	1.5		125	1.05	11.0
C8	0.23	0.278	0.90	1.3		74	1.05	9.50
C9	0.23	0.278	0.90	1.0		85	1.05	7.50

Lastly, we tried the polymerization with an excess of 5% of isatin. In general, reaction time remained short, and it led to a high gel formation and poor film forming properties of the polymer.

The optimization of the reaction had to be interrupted because there was no possibility to considerably increase the reaction time. The shorter the reaction time, the more decisive and difficult it was to identify the time in which the reaction must be quenched. No reaction was free from gel formation. An example of reaction with complete gel formation is shown in **Figure 4.6 (1)**.

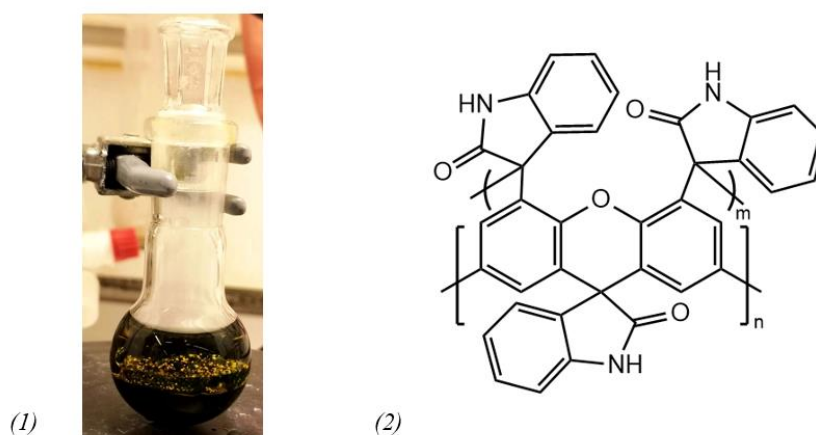


Figure 4.6 Polymer cross-linked (1) and possible structure (2).

A possible cross-linked structure is shown in **Figure 4.6 (2)**.

The molecular structure of the polymer was characterized by NMR spectroscopy, and the result is shown in **Figure 4.7 (a)**. The aromatic proton signals were found in the region between 6 and 8 ppm, which were difficult to distinguish from each other. The singlet located at 11 ppm corresponded to the amide proton. The nature of peaks between 9.5 and 10.8 ppm were not well determined. They were thought to be signals of hydroxyl protons influenced by strong hydrogen bonding. In spectrum **(b)** a small amount of TFA was added to the sample to eliminate acidic protons such as water and hydroxyl from the spectrum. In an acidic environment, the nitrogen atom will be present in the form of a quaternary ion, and therefore bound to two protons, visible in the spectrum at 10.9 and 10.45 ppm. There was also a peak around 9.8 ppm which disappeared after the addition of the acid. It was assumed that it was due to hydroxyl groups along the chain. This would mean that not all hydroxyl groups had managed to condense to give the ether bridge.

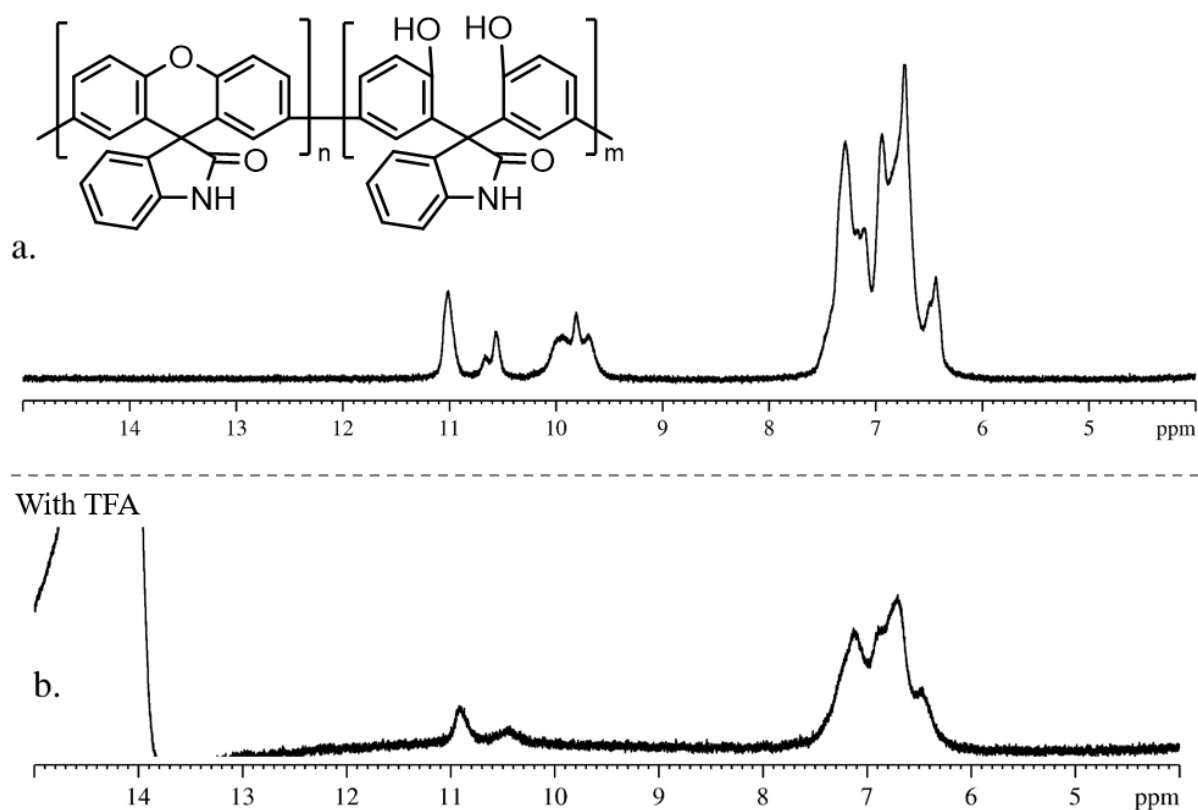


Figure 4.7 ¹H spectra of PSIX without (a) and with (b) TFA to eliminate acidic protons.

4.2.2 PBSIX

The NMR spectra of PBSIX and its structure are shown in **Figure 4.8**. The spectra were calibrated considering the aromatic signals account for ten protons. Signals from aliphatic

protons were observed. In spectrum (a) we can see that at 1.8 ppm there was a peak that integrates 4, corresponding to the 4 protons of the quintuplets $-CH_2-$, which had merged into a single peak. Between 3-4 ppm there were 3 peaks that integrate to 6. Two were due to the remaining $-CH_2-$ while the other was due to water, which had a peak at about 3.3. Between 9 and 10 ppm there were two peaks related to the presence of $-OH$ groups along the polymer chain. To shift the water signal, TFA was added to the sample. The spectrum of the sample with TFA is shown in **Figure 4.8 (b)**, and indicates that it was essential to shift the chemical shift of the water. We can observe how, after the addition, the integral of the aliphatic region counted 8 protons. Furthermore, the disappearance of the peaks at 9.6 ppm confirmed the presence of $-OH$ groups, while the broad peak remained at 9.6 was due to the protonated amine proton.

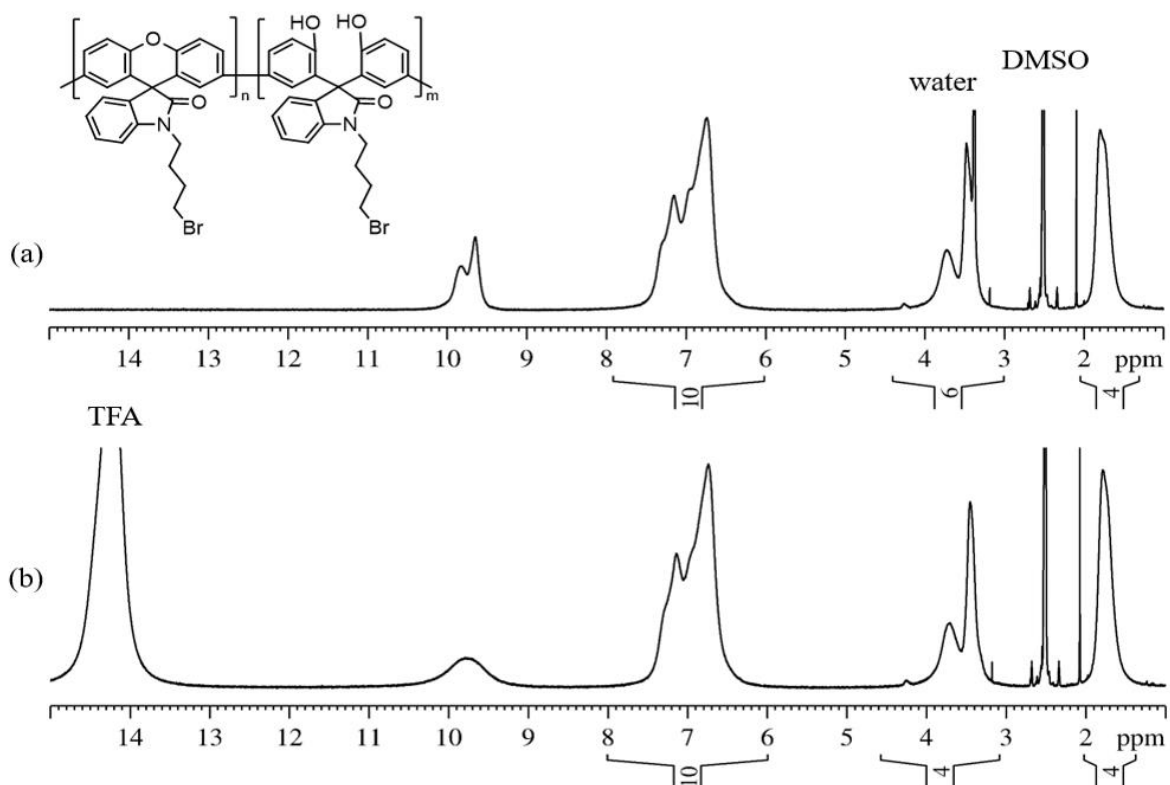


Figure 4.8 1H NMR spectra of PBSIX without (a) and with (b) TFA.

The first observation was a noticeable increase in the reaction time. The functionalization of isatin made the compound much less reactive than the non-functionalized one. The reaction conditions that produced the high quality polymer films consist of a 5% excess of monomer *D* over *B*, with a TFSA ratio between 10 and 11 equivalents. All the previous observations on colours and viscosity have also been found in this case (**Figure 4.9**). According to the literature, the increasing in viscosity assured the progression of the polymerization.

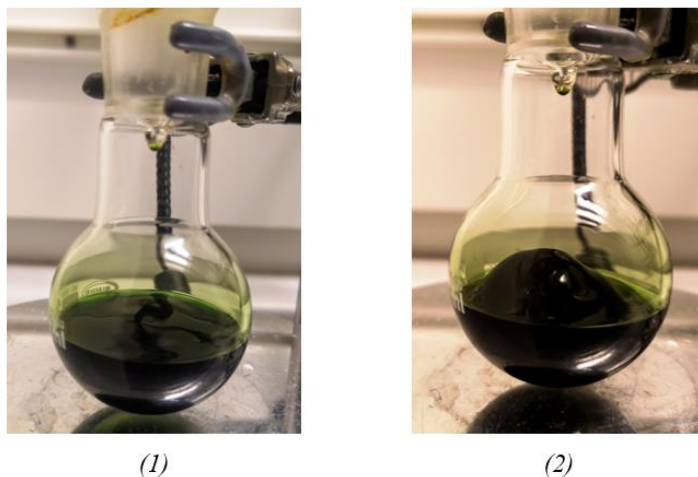


Figure 4.9 Solution after a few hours with low viscosity (1) and final solution with high viscosity (2).

Taking into consideration the NMR spectra of the polymer (**Figure 4.8**), a way was sought to eliminate the presence of the phenolic groups by changing the reaction conditions. To promote the condensation between phenolic groups were possible two options: increase the acidity of the solution or raise the temperature. A few small batches were made at 40 °C. However, the rise in temperature failed. In fact, the NMR analysis performed on the polymer obtained from the polymerization at high temperature did not show different peaks.

4.3 Quaternization

After the synthesis of the PBSIX, the quaternization reactions on the polymer were carried out. The polymer was dissolved in DMAc at 85°C, and the amine solution was then added. After the addition of the amine, a precipitation phenomenon of the polymer from the solution was observed after a few minutes, effectively preventing the desired reaction. **Figure 4.10** shows the precipitation of the polymer from the pyrrolidine solution.



Figure 4.10 Polymer precipitated (bottom) in NMP and pyrrolidine solution (top).

It was thought to be a solubility problem due to the solvent used, the dimethylacetamide (DMAc). In order to resolve that, the solvent was changed, using NMP, but the precipitation persisted. Analysis of the precipitate could have helped to understand what reaction was taking place, but the product was insoluble in common solvents for NMR. Generally, we can assume that a cross link reaction can occur in a basic environment. The TMA ($pK_a = 9.8$), the Pip ($pK_a = 10.1$) and the Pyr ($pK_a = 10.3$) are both strong bases and good nucleophiles.¹⁶¹ However, there were several chemical species present in the system. Factors contributing to the nucleophilicity of a species were: charge, electronegativity, solvent and steric hindrance. In aprotic solvents such as DMAc and NMP they did not give hydrogen bonds with the nucleophiles which therefore were less solvated and more reactive than they were in protic solvents. From NMR analyses we know that phenolic groups are present along the polymer chain. What most likely occurs is a deprotonation of these by the TMA to obtain a negatively charged form of the polymer (**Figure 4.11 (i)**). In this state, the bromine present in other molecules becomes a perfect leaving group (S_N2) which can react preferentially and faster with this new nucleophile. This leads to the cross link of the polymer (**ii**) which explains the precipitation.

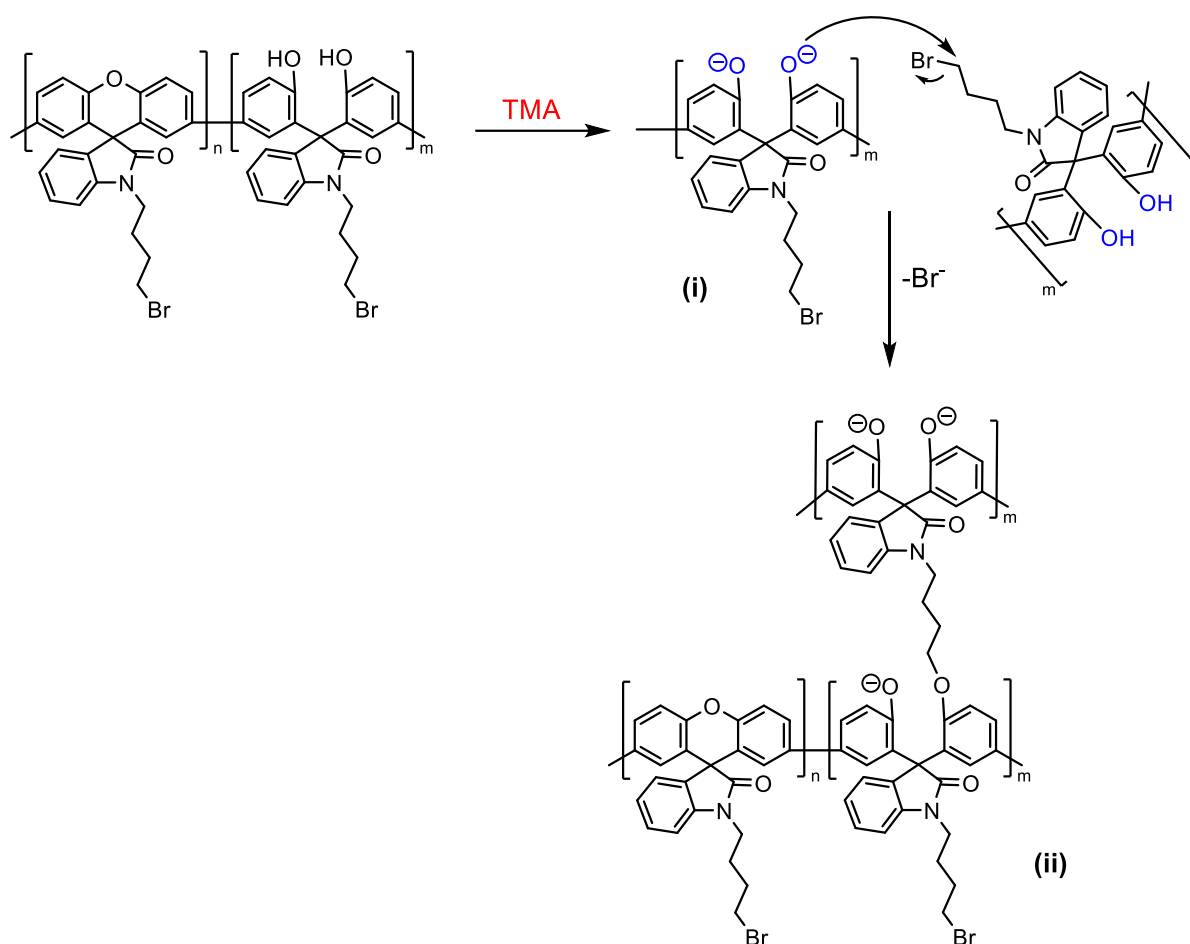


Figure 4.11 Cross link mechanism in basic conditions of PBSIX.

To overcome this obstacle it was necessary to think of a way to neutralize the phenolic groups and prevent this reaction from happening. One possible solution could be the methylation of OH- groups using, e.g., iodomethane (MeI). The polymer solution and iodomethane (50% excess) should be added to the reaction flask. Subsequently, a base capable of promoting the reaction, such as potassium carbonate (K_2CO_3), should be necessary added (**Figure 4.12**).

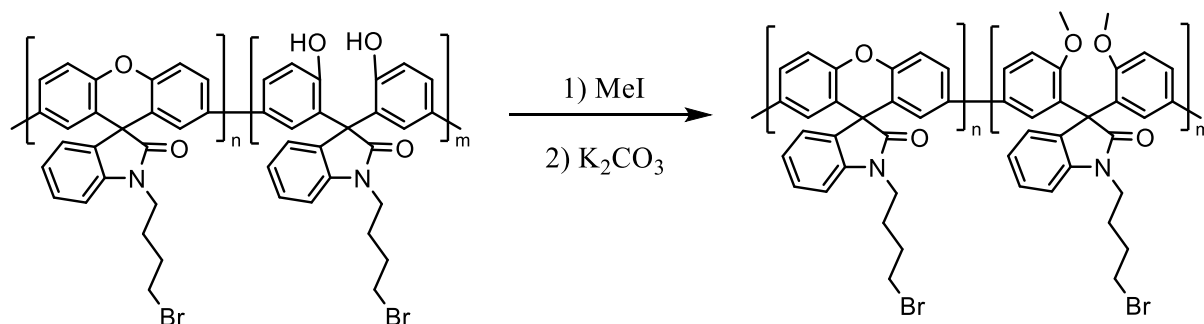


Figure 4.12 Methylation of the polymer in basic conditions.

4.4 Reaction mechanism

During the characterization, it was shown that the functional groups OH-, visible in the compound (**h**), did not always condense to give a compact structure through an oxygen ether bridge. This means that we cannot control the final structure of the polymer. Can we indicatively determine the extent of the phenomenon? We can formulate a hypothesis of what happens, and to do this we can approach the problem by analysing the mechanism starting from the tertiary carbocation (**1**) shown in 2D in **Figure 4.14**, or in a 3D version in **Figure 4.13 (1a)**.

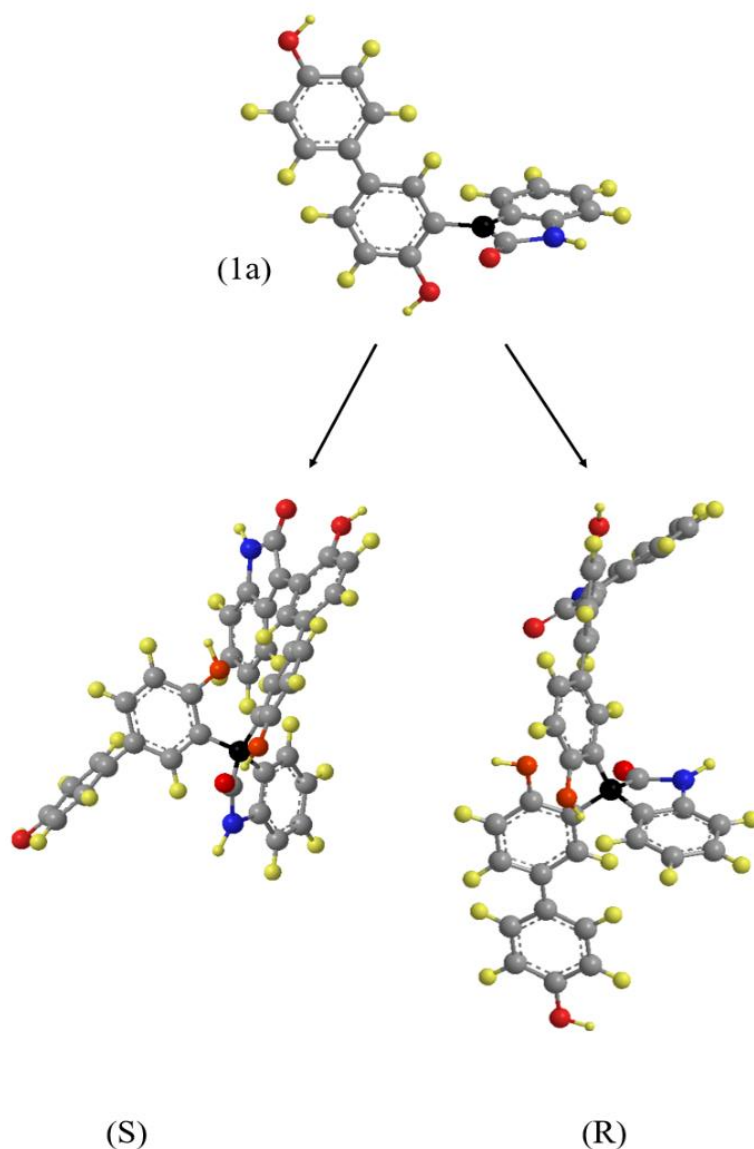


Figure 4.13 3D schematization of the planar carbocation (1a) and of the pair of enantiomeric compounds (S) and (R); groups involved in the mechanism highlighted in: -OH orange; C = O red; C black; N blue.

As generally a planar structure, carbocations may react at either of two faces.¹⁷⁴ As shown, the nucleophile can approach from behind (**2**) or frontally (**3**) in relation to the plane of the cation,

but with not the same probability and the product is a mixture of compounds (*S*) and (*R*). From **(1a)** we can see that there is a difference between the two faces. The lower one is sterically impeded by the presence of the isatin carbonyl and by the encumbrance of the biphenyl. The upper one, on the other hand, is more free and accessible. From the analysis of the NMR spectra it seems that the relationship between the two options is approximately 90/10 in favour of the less impeded face leading to the product (*S*). To understand why the (*R*) enantiomer can carry out the condensation reaction that leads to the product **(4)** while the one (*S*) is not, a 3D approach is essential, for this reason the models of the two enantiomers are also shown in **Figure 4.13**. The carbon highlighted in black is the one that undergoes the attack of the nucleophile while the oxygen atoms that are involved in the condensation are highlighted in orange. Taking the carbon plane as a reference point, in compound (*R*) we can observe that the two hydroxyl groups are close to each other, they are both in front of the plane and without any impediment between them. The carbonyl group (highlighted in red) points in the opposite direction and is behind the plane. This configuration allows the condensation of the two groups. The situation changes for the configuration (*S*). In this case, the carbonyl is located between the two groups, acting with a dual function as a steric and electrostatic impediment.

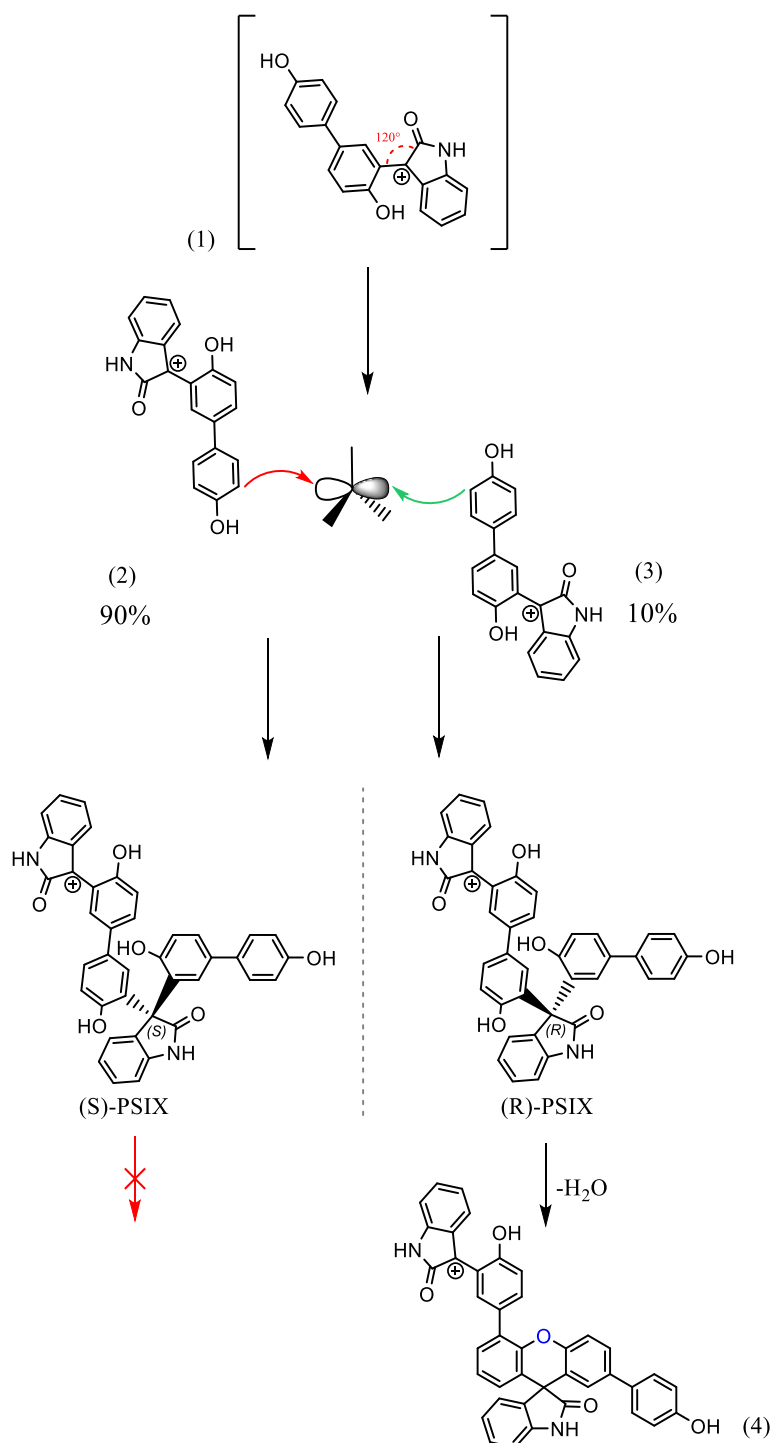


Figure 4.14 Mechanism of the reaction that leads to the formation of the (S) and (R) enantiomers.

However, the contribution made by isatin is not sufficient to explain the result obtained. To justify the chiral aspect of the mixture we need to take in consideration the use of hydroxybiphenyl. In fact, the steric conformation of the two rings prevents the free independent rotation of the two phenolic rings. In the literature there are examples of success both in the isatin-based polymers with hydroxyphenyls and 4,4'-dihydroxybiphenyl with electrophiles with

complete condensation.²³ **Figure 4.15** shows two examples of these. We can conclude that there is a sum of contributions, which includes, on the one hand, the impediment in the rotation of the nucleophile and, on the other, the ring system and the presence of the isatin carbonyl, which severely limit the possibility of condensation.

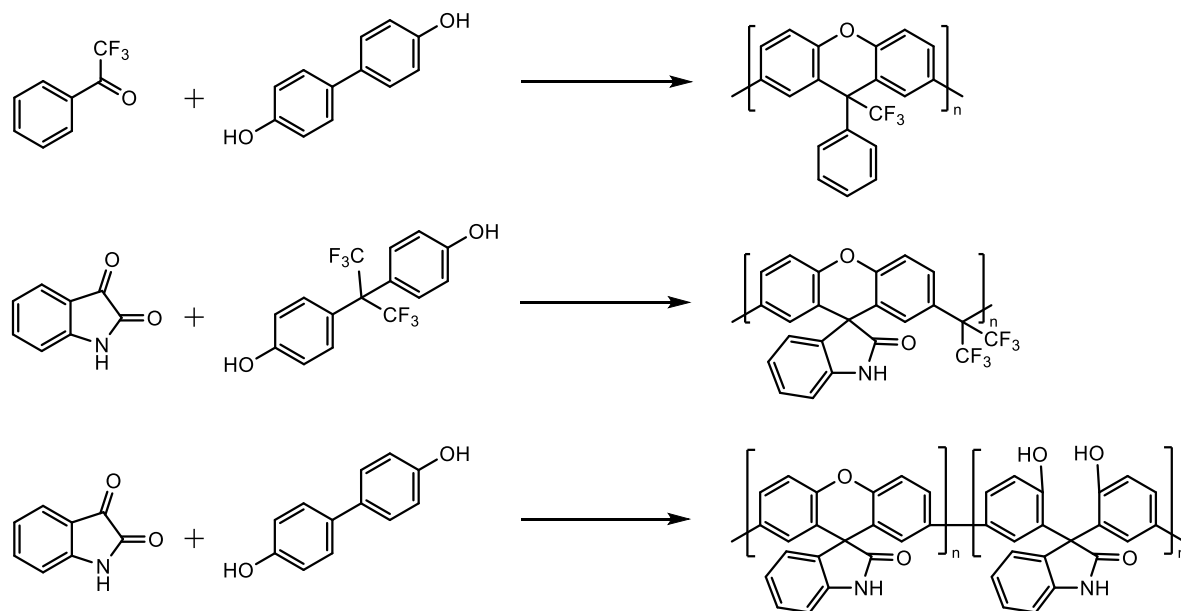


Figure 4.15 Examples of reactions where condensation is possible and partial.

4.5 Membrane characterizations

PSIX films:

All PSIX polymerizations resulted in a gel formation process. The consequence was that was very difficult to obtain polymer solutions without visible particles. **Figure 4.16 (a)** shows a film obtained in a fume hood from a 5 wt% solution (**Table 2**, A7), while **(b)** a film obtained from a 10 wt% solution (**Table 3**, B5).



Figure 4.16 Films of PSIX from casting of different solutions.

We can observe that the film forming properties of the synthesized polymer are quite low. The resulting films were of low quality. Mechanical properties were very poor, such as having great brittleness and almost no flexibility. The main causes of this result can be several. To begin with we can make a general consideration on the molecular weight of the polymer. With low MW, films loses its stability, the molecules pack up worse and are more distant, making the film brittle. On the contrary, high MW stabilize the film, favouring the chain entanglement and making the film more flexible. The goal should be the synthesis of the polymer with sufficient molecular weight to form good quality films. Furthermore, the polymer produced has multiple functional groups capable of establishing hydrogen bonds, such as C=O, -OH and -NH (**Figure 4.17**).

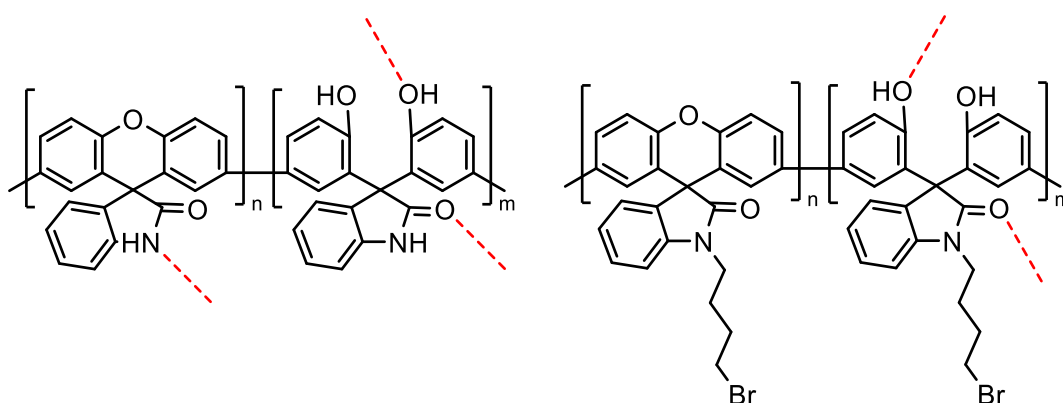


Figure 4.17 H bonds established between polymer chains.

A peculiar characteristic of the hydrogen bond is keeping the molecules concerned more distant from each other than the other types of bonds. Establishing these bonds can contribute to the weakening of films.

PBSIX films:

The method of preparation was the same as the one used for PSIX films. PBSIX films showed a higher quality (**Table 1**, entry 4) and it was possible to make more elastic films (**Figure 4.18 (b)**). In some cases, films showed a cracking phenomenon (**Table 1**, entry 1 and 5). It is thought that was due to the low molecular weight or a cooling of the film too fast. These micro fractures were highlighted with arrows in **Figure 4.18 (a)**.

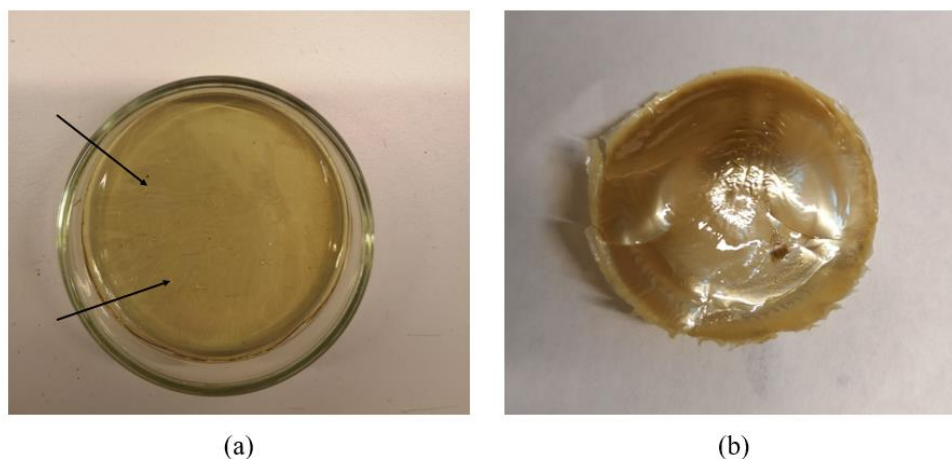


Figure 4.18 Films of PBSIX from casting of different solutions in DMF; in (a) micro-cracks in the film are indicated.

All the considerations about film forming properties and stability discussed above still applies to PBSIX. In addition, the use of BID was to make the polymer chains more flexible; butyl chains will act as a plasticizer, increasing the flexibility and improving film-forming properties.

4.6 SEC

One of the fastest and most practical methods of obtaining an indication of the molecular weight of the synthesized polymers was the SEC analysis. All the samples analysed were of PBSIX. In **Table 5** showed the synthesis (**Table 1**) and the corresponding MWs obtained. The peaks of the analysis were shown in **Figure 4.19**.

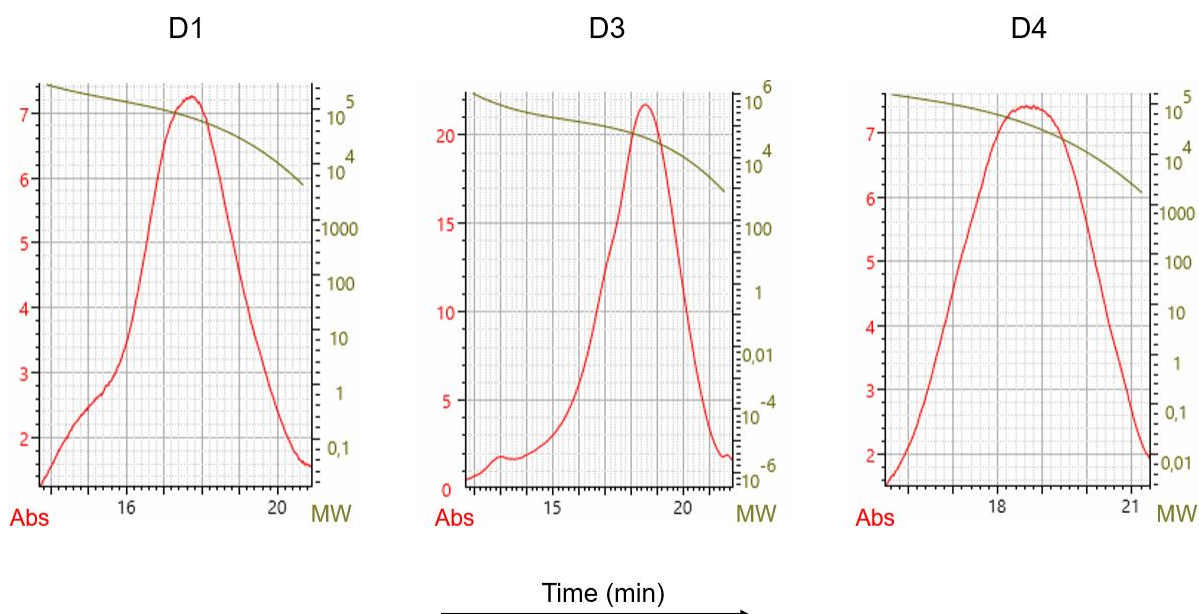


Figure 4.19 Chromatogram of three polymer samples; entries from Table 4.

From the data reported in the table for M_n and M_w we can conclude: in the analysed samples there were few long polymeric chains, but the majority were shorter in length.

Table 5 Molecular weight values and polydispersity of the analyzed samples

	M_n (kg/mol^1)	M_w (kg/mol^1)	PDI
D1	34000	89600	2.64
D3	21100	81600	3.86
D4	18600	48800	2.63

The reasons justifying these results were that the polymerization did not follow exactly the mechanism thought and produced high PDI and low MW chains. On the other hand, there was a possibility that the longer chains were not very soluble in THF, and during the solution filtration operation they cannot pass the filter.

4.7 TGA and DSC

The weight of the samples was continuously measured while increasing the temperature and the thermal decomposition temperature was taken after 5% weight loss ($T_{d,95}$). The thermogram is shown in **Figure 4.20**, while the decomposition temperatures and the residue weight % are listed in **Table 6**.

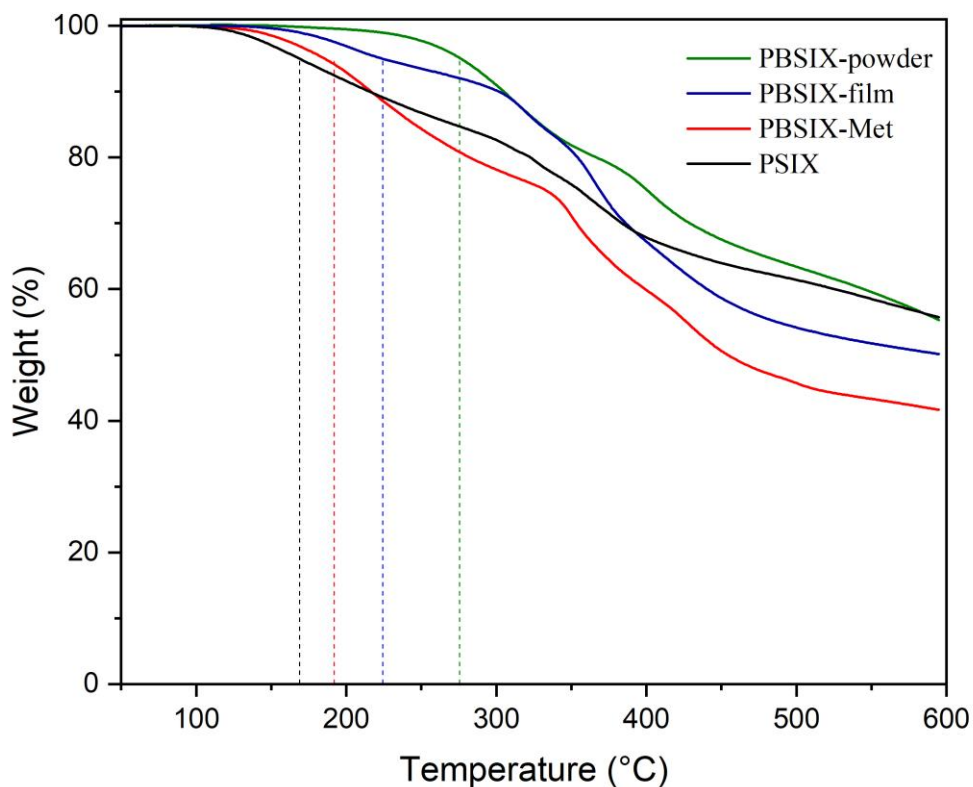


Figure 4.20 TGA curves of different samples of PBSIX and PSIX.

Table 6 Results of the thermogravimetric analysis of the polymer samples

<i>Entry</i>	<i>T_{d,95} °C</i>	<i>Residue wt %</i>
<i>PBSIX-powder</i>	224.2	50.2
<i>PBSIX-film</i>	275.5	55.2
<i>PBSIX-Met</i>	186.6	41.7
<i>PSIX</i>	168.9	60.1

DSC analysis involved heating the sample up to the polymer degradation temperature. However, the instrument detected no glass transition temperature (T_g) in the range analysed. From this result, we can conclude that the degradation temperature may be lower than the glass transition temperature.

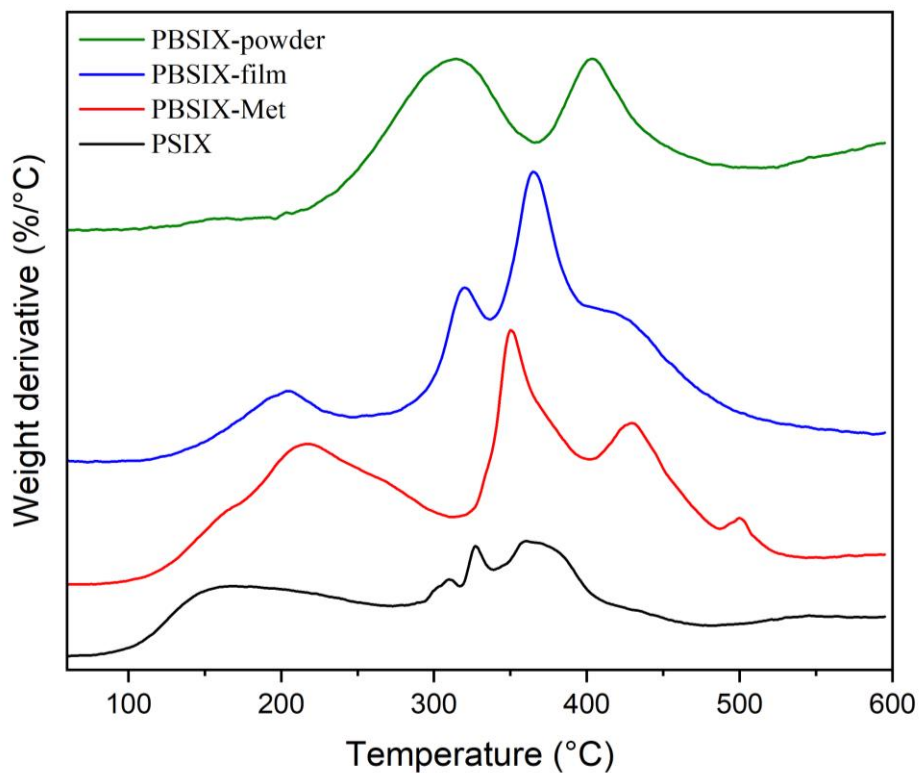


Figure 4.21 First derivative curves of the polymer samples from TGA analysis.

To observe the trend of the degradation phenomenon, in **Figure 4.21** were shown the curves of the first derivatives of the TGA analysis. The first shoulder, situated between 100 and 250 °C, represented the evaporation of the solvent remaining in the samples, e.g. DMSO at 190 °C. From the curves, we deduced that the decomposition was characterized by 3 steps. In the powder curve, the first peak was broadened and could have included two overlapping steps.

5 Conclusion and future outlook

In this thesis, it was intended to explore the possibility of using isatin-based polymers as membranes for separating gas mixtures and as quaternary ammonium functionalized anion exchange membranes.

The polymerizations studied in this work, with this specific pair of monomers, did not lead to the desired products, but to mixed products with structures shown in **Figure 5.1**. The synthesis and purification of the monomer derived from alkylated isatin was also investigated.

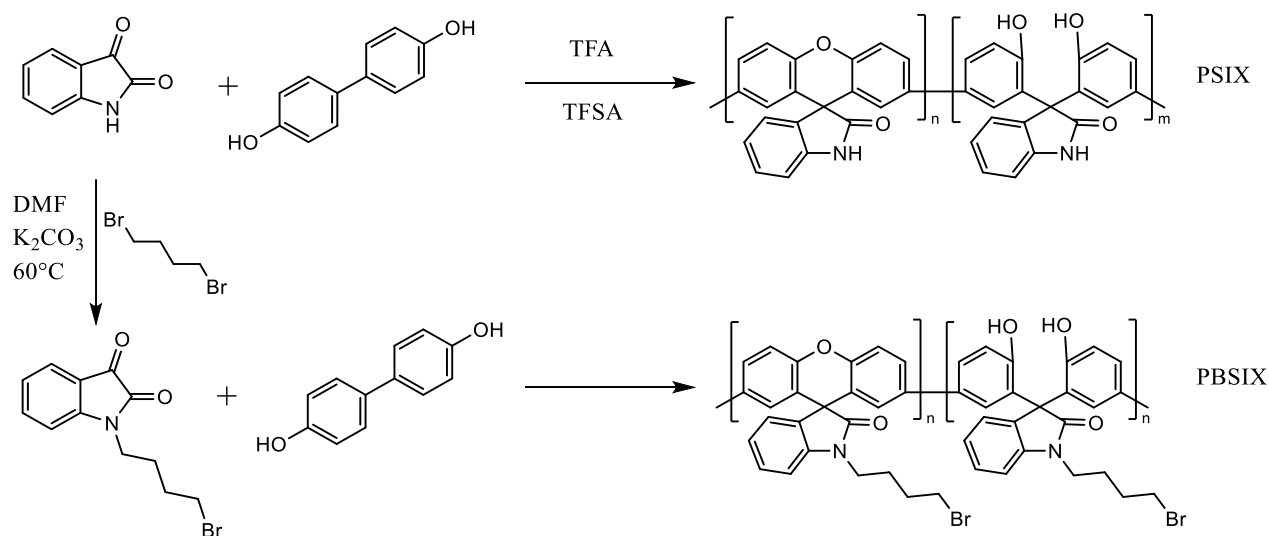


Figure 5.1 Synthetic routes for PSIX and PBSIX.

The PSIX polymer did not produce films that could be used for gas separation characterizations. At the same time, the functionalization reactions of PBSIX were not successful due to the phenolic groups along the polymer chains. During the reaction, a cross-link reaction occurred.

To overcome this problem, it is hypothetically possible to methylate the -OH and the -NH groups using, e.g., iodomethane (**Figure 5.2**). In this way, it is possible to avoid the crosslinking reaction, and the introduction of methyl groups does not enormously decrease the efficiency of the polymer in terms of free volume and gas separation properties.

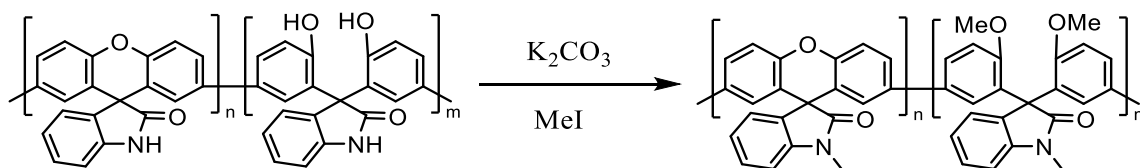


Figure 5.2 PSIX methylation reaction.

In the literature, these hydroxyl groups along the polymer chains are generally exploited for the synthesis of cation exchange membranes,^{40,175-177} which are functionalized with anions along the polymer. Since the percentage of condensation is less than or equal to 50%, it means that highly functionalized membranes could be synthesized thanks to the large amount of -OH. A general example involves the reaction shown in **Figure 5.3** that lead to sulphonic groups along the polymer.

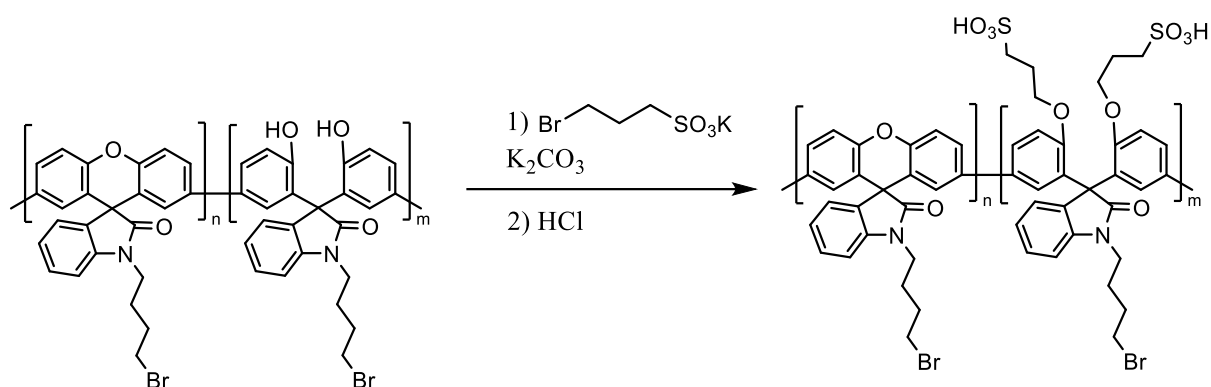


Figure 5.3 Synthesis of an anionic polymer for proton exchange membrane using PBSIX.

6 References

1. A. R. Cruz, M. C. G. Hernandez, M. T. Guzmán-Gutiérrez, M. G. Zolotukhin, S. Fomine, S. L. Morales, H. Kricheldorf, E. S. Wilks, J. Cárdenas, M. Salmón, *Macromolecules* **2012**, 45, 6774.
2. Jiménez Castillo, U.; Zolotukhin, M. G.; Fomina, L.; Romero Nieto, D.; Olivera Garza, L.; Fomine, S. *J. Mol. Model.* **2013**, 19, 793– 801.
3. Galasso, V.; Pellizer, G.; Pappalardo, G.C. *Org. Magn. Res.* **1977**, 9, 401.
4. Kreuer, K.-D., *Fuel Cells. Springer: New York*, **2013**.
5. Slade, R. C. T.; Kizewski, J. P.; Poynton, S. D.; Zeng, R.; Varcoe, J. R. *Ed. Springer New York: New York, NY*, **2013**; pp 9-29.
6. Wang, Y.; Chen, K. S.; Mishler, J.; Cho, S. C.; Adroher, X. C. *Appl. Energy* **2011**, 88, (4), 981-1007.
7. Franklin, G. W.; James, C. D. Fluorocarbon vinyl ether polymers, **1966**.
8. Scherer, G. G. Fuel Cell Types and Their Electrochemistry. In *Fuel Cells: Selected Entries from the Encyclopedia of Sustainability Science and Technology*, Kreuer, K.-D., Ed. Springer New York: New York, NY, **2013**; pp 97-119.
9. Merle, G.; Wessling, M.; Nijmeijer, K. J. *Membr. Sci.* **2011**, 377, (1–2), 1- 35.
10. Varcoe, J. R.; Slade, R. C. T. *Fuel Cells* **2005**, 5, (2), 187-200
11. Guzman-Gutierrez, M. T.; Nieto, D. R.; Fomine, S.; Morales, S.L.; Zolotukhin, M. G.; Hernandez, M. C. G.; Kricheldorf, H.; Wilks, E. S. *Macromolecules* **2011**, 44, 194–202.
12. Ran, J.; Wu, L.; He, Y.; Yang, Z.; Wang, Y.; Jiang, C.; Ge, L.; Bakangura, E.; Xu, T. J. *Membr. Sci.* **2017**, 522, 267-291.
13. Logan, B. E.; Elimelech, M. *Nature* **2012**, 488, 313.
14. D. R. Nieto, S. Fomine, M. G. Zolotukhin, L. Fomina, M. C. Gutiérrez, Hernandez, *Macromol. Theory Simul.* **2009**, 18, 138–144.
15. Zhang, H.; Shen, P. K. *Chem. Rev.* **2012**, 112, (5), 2780-2832.
16. Mansoor Namazian, Maryam Zakery, Mohammad R. Noorbala, Michelle L. Coote, *Elsevier*, **2007**.
17. Leng, Y.; Chen, G.; Mendoza, A. J.; Tighe, T. B.; Hickner, M. A.; Wang, C.-Y. *J. Am. Chem. Soc.* **2012**, 134, (22), 9054-9057.
18. Gu S, Cai R, Luo T, Chen Z, Sun M, Liu Y, He GH, Yan YS, *Angew Chem Int Ed* **2009**, 48:6499–502.
19. Dekel, D. R. J. *Power Sources* **2018**, 375, 158-169.

20. Varcoe, J. R.; Kizewski, J. P.; Halepoto, S. D.; Slade, R. C. T.; Zhao, F., *in Encyclopedia of Electrochemical Power Sources*, Garche, J.; Dyer, C. K., Eds. Elsevier: **2009**.
21. Wang, Y.; Chen, K. S.; Mishler, J.; Cho, S. C.; Adroher, X. C. *Appl. Energy* **2011**, 88, (4), 981-1007.
22. Juan Enrique Romero-Hernández, Alfredo Cruz-Rosado, Mikhail G. Zolotukhin, and Eduardo Vivaldo-Lima, *Macromolecular theory and simulations*, **2017**.
23. L. I. Olvera, M. G. Zolotukhin, O. Hernández-Cruz, S. Fomine, J. Cárdenas, R. L. Gaviño-Ramírez, F. A. Ruiz-Trevino, *ACS Macro Lett.* **2015**, 4, 492.
24. D. R. Nieto, M. G. Zolotukhin, L. Fomina, S. Fomine, *J. Phys. Org. Chem.* **2010**, 23, 878.
25. Olah, G. A., Surya Prakash, G. K.; Molnar, A.; Sommer, J. *Superacid Chemistry, 2nd ed.*, Wiley & Sons: Hoboken, NJ, **2009**; Chapter 5, p501-750.
26. Klumpp, D. A.; Yeung, K. Y.; Prakash, G. K. S.; Olah, G. A. *J. Org. Chem.* **1998**, 63, 4481–4484.
27. Colquhoun, H.M.; Zolotukhin, M.G.; Khalilov, L.M.; Dzhemilev, U. M. *Macromolecules* **2001**, 34, 1122–1124.
28. Slade, R. C. T.; Kizewski, J. P.; Poynton, S. D.; Zeng, R.; Varcoe, J. R., *Selected Entries from the Encyclopedia of Sustainability Science and Technology*, Kreuer, K.-D., Ed. Springer New York: New York, NY, **2013**; pp 9-29.
29. Scherer, G. G. Fuel Cell Types and Their Electrochemistry. In *Fuel Cells: Selected Entries from the Encyclopedia of Sustainability Science and Technology*, Kreuer, K.-D., Ed. Springer New York: New York, NY, **2013**; pp 97-119.
30. Poynton, S. D.; Kizewski, J. P.; Slade, R. C. T.; Varcoe, J. R. *Solid State Ionics* **2010**, 181, 219-222.
31. Jasinski, R. *Nature* **1964**, 201, 1212-1213.
32. Wu, Q.; Jiang, L.; Tang, Q.; Liu, J.; Wang, S.; Sun, G. *Electrochim. Acta* **2013**, 91, 314-322.
33. Gu, S.; Sheng, W.; Cai, R.; Alia, S. M.; Song, S.; Jensen, K. O.; Yan, Y. *Chem. Commun.* **2013**, 49, 131-133.
34. Varcoe, J. R.; Atanassov, P.; Dekel, D. R.; Herring, A. M.; Hickner, M. A.; Kohl, P. A.; Kucernak, A. R.; Mustain, W. E.; Nijmeijer, K.; Scott, K.; Xu, T.; Zhuang, L. *Energy Environ. Sci.* **2014**, 7, 3135-3191.
35. Ohyama, J.; Okata, Y.; Watabe, N.; Katagiri, M.; Nakamura, A.; Arikawa, H.; Shimizu, K.-i.; Takeguchi, T.; Ueda, W.; Satsuma, A. *J. Power Sources* **2014**, 245, 998-1004.
36. Marino, M. G.; Kreuer, K.-D. *ChemSusChem* **2015**, 8, (3), 513-523.

37. Hickner, M. A.; Herring, A. M.; Coughlin, E. B. J. *Polym. Sci., Part B: Polym. Phys.* **2013**, 51, (24), 1727-1735.
38. Hugar, K. M.; You, W.; Coates, G. W. *ACS Energy Lett.* **2019**, 4, (7), 1681-1686.
39. Marino, M. G.; Melchior, J. P.; Wohlfarth, A.; Kreuer, K. D. J. *Membr. Sci.* **2014**, 464, 61-71.
40. Taewook R., Faiz A., Sabuj Chandra S., Nasrin S. L., Hanmo Y., Soojin Y., Seungchan L., Inhwan C., Whangi Ki., *Int. J. of Hydrogen Energy*, Volume 43, **2018**, Pag. 11862-11871.
41. Dekel, D. R.; Willdorf, S.; Ash, U.; Amar, M.; Pusara, S.; Dhara, S.; Srebnik, S.; Diesendruck, C. E. *J. Power Sources* **2018**, 375, 351-360.
42. Tuckerman, M. E.; Marx, D.; Parrinello, M. *Nature* **2002**, 417, (6892), 925- 929
43. de Grotthuss, C. *Ann. Chim.* **1806**, 58, 54-74.
44. Chen, M.; Zheng, L.; Santra, B.; Ko, H.-Y.; DiStasio Jr, R. A.; Klein, M. L.; Car, R.; Wu, X. *Nat. Chem.* **2018**, 10, (4), 413-419.
45. Marx, D.; Chandra, A.; Tuckerman, M. E. *Chem. Rev.* **2010**, 110, 2174- 2216.
46. Peckham, T. J.; Holdcroft, S. *Adv. Mater.* **2010**, 22, 4667-4690
47. Vandiver, M. A.; Caire, B. R.; Carver, J. R.; Waldrop, K.; Hibbs, M. R.; Varcoe, J. R.; Herring, A. M.; Liberatore, M. W. J. *Electrochem. Soc.* **2014**, 161, H677-H683.
48. Edson, J. B.; Macomber, C. S.; Pivovar, B. S.; Boncella, J. M. J. *Membr. Sci.* **2012**, 399 400, 49-59.
49. Chempath, S.; Einsla, B. R.; Pratt, L. R.; Macomber, C. S.; Boncella, J. M.; Rau, J. A.; Pivovar, B. S. *Journal of Physical Chemistry C* **2008**, 112, 3179- 3182.
50. Cerichelli, G.; Illuminati, G.; Lillocci, C. *The Journal of Organic Chemistry* **1980**, 45, 3952-3957.
51. Cope, A. C.; Mehta, A. S. *J. Am. Chem. Soc.* **1963**, 85, 1949-1952
52. Chempath, S.; Boncella, J. M.; Pratt, L. R.; Henson, N.; Pivovar, B. S. *The Journal of Physical Chemistry C* **2010**, 114, 11977-11983.
53. Archer, D. A. *Journal of the Chemical Society C: Organic* **1971**, 1329-1331.
54. Kantor, S. W.; Hauser, C. R. *J. Am. Chem. Soc.* **1951**, 73, 4122-4131.
55. Mohanty, A. D.; Tignor, S. E.; Krause, J. A.; Choe, Y. K.; Bae, C. *Macromolecules* **2016**, 49, 3361-3372
56. Miyanishi, S.; Yamaguchi, T. *PCCP* **2016**, 18, 12009-12023.
57. Amel, A.; Zhu, L.; Hickner, M.; Ein-Eli, Y. J. *Electrochem. Soc.* **2014**, 161, F615-F621.
58. Fujimoto, C.; Kim, D.-Sc.; Hibbs, M.; Wroblewski, D.; Kim, Y. S. *J. Membr. Sci.* **2012**, 423-424, 438-449.

59. Choe, Y.-K.; Fujimoto, C.; Lee, K.-S.; Dalton, L. T.; Ayers, K.; Henson, N. J.; Kim, Y. S. *Chem. Mater.* **2014**, 26, 5675-5682.
60. Thomas, O. D.; Soo, K. J.; Peckham, T. J.; Kulkarni, M. P.; Holdcroft, S. J. *Am. Chem. Soc.* **2012**, 134, 10753-6.
61. Hugar, K. M.; Kostalik, H. A.; Coates, G. W. *J. Am. Chem. Soc.* **2015**, 137, 8730-8737.
62. Mohanty, A. D.; Bae, C. *Journal of Materials Chemistry* **2014**, 2, 17314- 17320.
63. Lee, W.-H.; Mohanty, A. D.; Bae, C. *ACS Macro Letters* **2015**, 4, 453-457.
64. Yang, Z.; Zhou, J.; Wang, S.; Hou, J.; Wu, L.; Xu, T. *Journal of Materials Chemistry A* **2015**, 3, 15015-15019.
65. Liu, Y.; Zhang, B.; Kinsinger, C. L.; Yang, Y.; Seifert, S.; Yan, Y.; Mark Maupin, C.; Liberatore, M. W.; Herring, A. M. *J. Membr. Sci.* **2016**, 506, 50-59.
66. Wang, J.; Li, S.; Zhang, S. *Macromolecules* **2010**, 43, 3890-3896.
67. Miyake, J.; Fukasawa, K.; Watanabe, M.; Miyatake, K. *J. Polym. Sci., Part A: Polym. Chem.* **2014**, 52, 383-389.
68. Qu, C.; Zhang, H.; Zhang, F.; Liu, B. *J. Mater. Chem.* **2012**, 22, 8203-8207.
69. Liu, L.; Li, Q.; Dai, J.; Wang, H.; Jin, B.; Bai, R. *J. Membr. Sci.* **2014**, 453, 52-60.
70. Li, Y.; Xu, T.; Gong, M. *J. Membr. Sci.* **2006**, 279, 200-208.
71. You, W.; Noonan, K. J. T.; Coates, G. W. *Prog. Polym. Sci.* **2020**, 100, 101177.
72. D. Dekel, Alkaline membrane fuel cells, in *Encyclopedia of Applied Electrochemistry*, Springer Reference number 303632, **2014**.
73. Yampolskii Y., *Advanced Membrane Science and Technology for Sustainable Energy and Environmental Applications*, Woodhead Publishing Series in Energy, **2011**, Pages 22-55.
74. Boeddeker K. W., 'Commentary tracing membrane science', **1995**, *J Membr Sci*, Special Issue, 100, 1-68.
75. von Wroblewski S., *Ann Physik u Chem* , **1879**, 8, 29-52.
76. J. Crank, *The Mathematics of Diffusion*, Clarendon Press, Oxford, **1975**.
77. H.K. Lonsdale, *J Membr Sci*, 43, **1989**, pp. 1-3.
78. P. Meares, *Encyclopedic Dictionary of Physics*, 4, Pergamon Press, Oxford **1961**, p. 561.
79. R.W. Baker, *Concise Encyclopedia of Polymer Science and Technology* (third edition), Wiley, Hoboken **2007**, p. 657.
80. S. Matteucci, Yampolskii Yu., B.D. Freeman and I. Pinnau, Yampolskii Yu., I. Pinnau, B.D. Freeman (Eds.), *Materials Science of Membranes for Gas and Vapor Separation*, Wiley, Chichester **2006**, p. 1.

- 81.** L.A. Pilato, L.M. Litz, B. Haritay, A.G. Farnham, J.H. Kawakami, P.E. Fritze and J.E. McGrath, Am Chem Soc Div Polym Chem, Polym Preprints, 16 **1975**, pp. 41-46.
- 82.** A.J. Kilpatrick, Some relations between molecular structure and plasticizing effect, *J. Appl. Phys.* 11 **1940**, 255-261.
- 83.** F.W. Clark, Plasticizers Soc. of Chem. Ind. e J. Chem. Ind., vol. 60, **1941**, pp. 225-228.
- 84.** R. Houwink, Proc. XI Cong. Pure Appl. Chem., London, **1947**, pp. 575-583.
- 85.** D.F. Cadogan, C.J. Howick, in: Kirk-Othmer (Ed.), Encyclopedia of Chemical Technology, John Wiley and Sons, New York, **1996** (Chapter: "Plasticizers").
- 86.** W. Aiken, T. Alfrey, A. Janssen, H. Mark, Creep behavior of plasticized vinylite VYNW, *J. Polym. Sci.* 2 **1947**, 178-198.
- 87.** Ewa Langer, Krzysztof Bortel, Sylwia Waskiewicz, Marta Lenartowicz-Klik, Plasticizers Derived from Post-Consumer PET, **2020**, Pages 1-11.
- 88.** Flory P J, *J. Am. Chem. Soc.*, 62, 1057, **1940**.
- 89.** Fox T G, Flory P J, *J. Am. Chem. Soc.*, 70, 2384, **1948**.
- 90.** Ueberreiter K, Kanig G, *J. Colloid Sci.*, 7, 569, **1952**.
- 92.** Fox T G, Flory P J, *J. Appl. Phys.*, 21, 581, **1950**.
- 93.** Ferry J D, Viscoelastic Properties of Polymers, 3rd Ed., Wiley, New York, **1980**.
- 94.** Cohen, M. H.; Turnbull, D. *J. Chem. Phys.* **1959**, 31, 1164–1169.
- 95.** Brandt, W. *Phys. Rev.* **1955**, 98, 243.
- 96.** DiBenedetto, A. T. *J. Polym. Sci. Part A* **1963**, 1, 3477–3487.
- 97.** Pace, R. J.; Datyner, A. J. *Polym. Sci. Part B: Polym. Phys.*, **1979**, 17, 437–451.
- 98.** L. M. Robeson, *J. Membr. Sci.* **2008**, 320, 390–400.
- 99.** L.M. Robeson, Correlation of separation factor versus permeability for polymeric membranes, *J. Membr. Sci.* 62 **1991**, 165.
- 100.** L.M. Robeson, W.F. Burgoyne, M. Langsam, A.C. Savoca, C.F. Tien, *Polymer* 35 **1994**, 4970.
- 101.** B.D. Freeman, *Macromolecules* 32 **1999**, 375.
- 102.** J.Y. Park, D.R. Paul, *J. Membr. Sci.* 125 **1997**, 23.
- 103.** L.M. Robeson, C.D. Smith, M. Langsam, *J. Membr. Sci.* 132 **1997**, 33.
- 104.** D.V. Laciak, L.M. Robeson, C.D. Smith, Group contribution modeling of gas transport in polymeric membranes, in: B.D. Freeman, I. Pinnau (Eds.), ACS Symposium Series 733, American Chemical Society, Washington, DC, **1999**, p. 151.
- 105.** Joaquim F. M. da Silva, Simon J. Garden and Angelo C. Pinto, *J. Braz. Chem. Soc.*, Vol. 12, No. 3, 273-324, **2001**.

- 106.** Alfredo Cruz-Rosado, Juan Enrique Romero-Hernández, Marlene Ríos-López, Salvador López Morales, Gerardo Cedillo, Lucero Mayra Ríos-Ruiz, Enoc Cetina- Mancilla, Joaquín Palacios Alquisira, Mikhail G. Zolotukhin, Eduardo Vivaldo-Lima, *Polymer*, **2022**.
- 107.** Ziqin Li, Riming Yu, Chang Liu , Jifu Zheng, Jing Guo , Tauqir A. Sherazi, Shenghai Li, Suobo Zhang, *Elsevier, Polymer 222*, **2021**.
- 108.** Aleksander Trummal,, Lauri Lipping, Ivari Kaljurand, Ilmar A. Koppel, and Ivo Leito, J. *Phys. Chem. A*. **2016**, 120, 3663-3669.
- 109.** E. L. Eliel, “Stereochemistry of Carbon Compounds”, McGraw-Hill, New York **1962**.
- 110.** G. A. Olah, *Angew. Chem. Int. Ed.* **1993**, 32, 767.
- 112.** <https://www.agilent.com>
- 113.** Synge, R. L. M., Teselius, A., *Biochemical Journal* **1950**, 46.
- 114.** Cytiva, Principles and methods Size Exclusion Chromatography.
- 115.** Cowie, J. M. G.; Arrighi, V. *Polymers: Chemistry and Physics of Modern Materials, Third Edition*. CRC Press: **2007**.
- 116.** Zhou, J.; Unlu, M.; Vega, J. A.; Kohl, P. A. *J. Power Sources* **2009**, 190, (2), 285-292.
- 117.** Zhang, F.; Zhang, H.; Qu, C. *J. Mater. Chem.* **2011**, 21, (34), 12744-12752.
- 118.** Arges, C. G.; Ramani, V. *Proc. Natl. Acad. Sci. U.S.A.* **2013**, 110, (7), 2490-2495.
- 119.** Weiber, E. A.; Jannasch, P. *ChemSusChem* **2014**, 7, (9), 2621-2630.
- 120.** Chen, D.; Hickner, M. A. *ACS Applied Materials & Interfaces* **2012**, 4, (11), 5775-5781.
- 121.** Weiber, E. A.; Meis, D.; Jannasch, P. *Polymer Chemistry* **2015**, 6, (11), 1986-1996.
- 122.** Amel, A.; Zhu, L.; Hickner, M.; Ein-Eli, Y. *J. Electrochem. Soc.* **2014**, 161, F615-F621.
- 123.** Dang, H.-S.; Jannasch, P. *Journal of Materials Chemistry A* **2016**, 4, 11924-11938.
- 124.** Yang, Z.; Guo, R.; Malpass-Evans, R.; Carta, M.; McKeown, N. B.; Guiver, M. D.; Wu, L.; Xu, T. *Angew. Chem. Int. Ed.* **2016**, 55, 11499-11502.
- 125.** Dang, H.-S.; Jannasch, P. *Journal of Materials Chemistry A* **2017**, 5, 21965-21978.
- 126.** Hahn, S.-J.; Won, M.; Kim, T.-H. *Polym. Bull.* **2013**, 70, 3373-3385.
- 127.** Morandi, C. G.; Peach, R.; Krieg, H. M.; Kerres, J. *Journal of Materials Chemistry A* **2015**, 3, 1110-1120.
- 128.** Akiyama, R.; Yokota, N.; Miyatake, K. *Macromolecules* **2019**, 52, (5), 2131-2138.
- 129.** Wright, A. G.; Weissbach, T.; Holdcroft, S. *Angew. Chem. Int. Ed.* **2016**, 55, (15), 4818-4821.
- 130.** Hibbs, M. R. *J. Polym. Sci., Part B: Polym. Phys.* **2013**, 51, (24), 1736-1742.
- 131.** Hibbs, M. R.; Fujimoto, C. H.; Cornelius, C. J. *Macromolecules* **2009**, 42, (21), 8316-8321.

132. Lee, W.-H.; Park, E. J.; Han, J.; Shin, D. W.; Kim, Y. S.; Bae, C. *ACS Macro Lett.* **2017**, 6, (5), 566-570.
133. Lee, W.-H.; Kim, Y. S.; Bae, C. *ACS Macro Lett.* **2015**, 4, (8), 814-818.
134. Wang, J.; Zhao, Y.; Setzler, B. P.; Rojas-Carbonell, S.; Ben Yehuda, C.; Amel, A.; Page, M.; Wang, L.; Hu, K.; Shi, L.; Gottesfeld, S.; Xu, B.; Yan, Y. *Nat. Energy* **2019**.
135. Olsson, J. S.; Pham, T. H.; Jannasch, P. *J. Membr. Sci.* **2019**, 578, 183-195.
136. Pham, T. H.; Olsson, J. S.; Jannasch, P. *J. Mater. Chem. A* **2019**.
137. Pham, T. H.; Olsson, J. S.; Jannasch, P. *J. Mater. Chem. A* **2018**, 6, (34), 16537-16547.
138. Olsson, J. S.; Pham, T. H.; Jannasch, P. *Adv. Funct. Mater.* **2017**, 28, 1702758.
139. Peng, H.; Li, Q.; Hu, M.; Xiao, L.; Lu, J.; Zhuang, L. *J. Power Sources* **2018**, 390, 165-167.
140. Ren, R.; Zhang, S.; Miller, H. A.; Vizza, F.; Varcoe, J. R.; He, Q. *ACS Appl. Energy Mater.* **2019**, 2, (7), 4576-4581.
141. Fan, J.; Wright, A. G.; Britton, B.; Weissbach, T.; Skalski, T. J. G.; Ward, J.; Peckham, T. J.; Holdcroft, S. *ACS Macro Lett.* **2017**, 1089-1093.
142. Long H, Pivovar B., *J Phys Chem C* **2014**;118:9880–8.
143. M. Tomoi, K. Yamaguchi, R. Ando, Y. Kantake, Y. Aosaki, H. Kubota, *J. Appl. Polym. Sci.* **1997**, 64, 1161-1167.
144. N. Li, T. Yan, Z. Li, T. Thurn-Albrecht, W. H. Binder, *Energy Environ. Sci.* **2012**, 5, 7888-7892.
145. Sun Z, Pan J, Guo J, Yan F., *Adv Sci* **2018**;
146. Lee B, Yun D, Lee J-S, Park CH, Kim T-H, *J Phys Chem C* **2019**;123:13508–18.
147. Liu Y, Wang J, Yang Y, Brenner TM, Seifert S, Yan Y, MW, *J Phys Chem C* **2014**;118:15136–45
148. Han H, Ma H, Yu J, Zhu H, Wang Z., *Eur Polym J* **2019**;114:109–17.
149. Noonan KJ, Hugar KM, Kostalik HAt, Lobkovsky EB, Abruna HD, Coates GW., *J Am Chem Soc* **2012**;134:18161–4.
150. Zhang B, Gu S, Wang J, Liu Y, Herring AM, Yan Y., *RSC Adv* **2012**;2:12683–5.
151. Zha Y, Disabb-Miller ML, Johnson ZD, Hickner MA, Tew GN., *J Am Chem Soc* **2012**;134:4493–6.
152. Gu S, Wang J, Kaspar RB, Fang Q, Zhang B, Coughlin EB, Yan Y., *Sci Rep* **2015**;5 11668/1-11.
153. Chen N, Zhu H, Chu Y, Li R, Liu Y, Wang F., *Polym Chem* **2017**;8:1381–92.

- 154.** Kwasny MT, Zhu L, Hickner MA, Tew GN, *J Polym Sci Part A Polym Chem* **2018**;56:328–39.
- 155.** G. Cerichelli, G. Illuminati, C. Lillocci, *J. Org. Chem.* **1980**, 45, 3952 – 3957.
- 156.** G. Illuminati, C. Lillocci, *J. Org. Chem.* **1977**, 42, 2201 – 2203.
- 157.** G. Cospito, G. Illuminati, C. Lillocci, H. Petride, *J. Org. Chem.* **1981**, 46, 2944 – 2947.
- 158.** M. Smith, J. March, March's Advanced Organic Chemistry: Reactions, Mechanisms, and Structure, Wiley, Hoboken, NJ, **2007**.
- 159.** K. A. Cooper, E. D. Hughes, C. K. Ingold, B. J. MacNulty, *J. Chem. Soc.* **1948**, 2049-2054.
- 160.** Meier-Haack, J.; Taeger, A.; Vogel, C.; Schlenstedt, K.; Lenk, W.; Lehmann, D. *Sep. Purif. Technol.* **2005**, 41, 207-220.
- 161.** Settimo, L., Bellman, K. & Knechtel, R.M.A. Comparison of the Accuracy of Experimental and Predicted pKa Values of Basic and Acidic Compounds. *Pharm Res* 31, 1082–1095, **2014**.
- 162.** Dang Hai-Son and Jannasch Patric, *Journal of Materials Chemistry A* 5(41), p.21965-21978, **2017**.
- 163.** <https://sites.unimi.it/ECEA/0910Impedenza.pdf>
- 164.** P. Vadhva, J. Hu, M. J. Johnson, R. Stocker, M. Braglia, D. J. L. Brett and A. J. E. Rettie, *ChemElectroChem*, **2021**, 8, 1930-1947.
- 165.** A. J. Bard and L. R. Faulkner, John Wiley & Sons, New York, **1980**, ch. 9, pp. 316-324.
- 166.** Y. Pu, Z. Dong, P. Zhang, Y. Wu, J. Zhao and Y. Luo, *J. Alloys Compd.*, **2016**, 672, 64-71.
- 167.** B. Huber, T. Linder, K. Hormann, T. Frömling, J. Sundermeyer and B. Roling, *Z. Phys. Chem.*, **2012**, 226, 377-390.
- 168.** X. Cai, B. Ye, J. Ding, Z. Chi, L. Sun, P. Saha and G. Wang, *J. Mater. Chem. A*, **2021**, 9, 2459-2469.
- 169.** H. H. Singh and H. B. Sharma, *Solid State Commun.*, **2020**, 319,114012.
- 170.** V. Senthil, T. Badapanda, S. N. Kumar, P. Kumar and S. Panigrahi, *J. Polym. Res.*, **2012**, 19, 9838.
- 171.** M. Faridi, L. Naji, S. Kazemifard and N. Pourali, *Chemical Papers*, **2018**, 72, 2289-2300.
- 172.** Bruce, P. G. In Polymer Electrolyte Reviews 1; MacCallum, J. R., Vincent, C. A., Eds; Essex, England, **1987**, p 237-270.
- 173.** I. Chiyanzu, C. Clarkson, P. J. Smith, J. Lehman, J. Gut, P. J. Rosenthal and K. Chibale, *Bioorg. Med. Chem.*, **2005**, 13, 3249–3261.
- 174.** Rajasekhar R. N. and Douglas A. Klumpp, *Chem. Rev.* 2013, 113, 9, 6905–6948, **2013**.

- 175.** Youngdon Lim, Soonho Lee, Hohyoun Jang, Taehoon Hong, Jiho Yoo, Jaeseong Ha, Donghoon Lee, Whangi Kim, *Int. J. of Hydrogen Energy*, Vol. 39, **2014**, Pag. 21613-21619,
- 176.** Youngdon L., Soonho L., Hohyoun J., Md. Awlad H., Seongyoung Choi, Younggil Cho, Jinseong Lim, Whangi Kim, *Renewable Energy*, Volume 79, **2015**, Pag. 85-90.
- 177.** Hohyoun J., Jaeseong Ha, Jiho Yoo, J. P., Chaekyun L., Taewook R., Kunyoung C., Whangi K., *Int. J. of Hydrogen Energy*, Volume 41, **2016**, Pag. 10466-10472.

7 Acknowledgements

This thesis has been performed at the Centre for Analysis and Synthesis (CAS) at Lund University. This Erasmus period meant a lot to me. It is my first real experience abroad and I am happy that it was here. Although I only spent a few months in Sweden, I have experienced many moments of despair and happiness. For these reasons, I would like to give warm thanks to people who have helped and supported me in this adventure.

First of all, I would like to thank Patric Jannasch, without whom I would not have been able to be here. One of the things I am most grateful for is how you provided guidance to follow, while allowing me to perform my project independently.

A big thanks goes to my supervisor Dong. I walked into the laboratory the first day knowing next to nothing about this field and she was the person who taught me most of the things I know. I think she had to have a lot of patience with me, considering all the times I went to bother her with questions.

A special thanks go to my colleagues who had the misfortune to share the lab with me, Si and Andrit. The chats with Andrit in the laboratory and in the cafeteria about Italy and Albania will always be with me. A special thanks goes to Si, who despite not having to help me was fundamental in my laboratory work. Countless times his help has saved me weeks of delay.

Lastly, to all past and present members of the polymer electrolyte membrane research group, a big thank you!

I thank my roommate Chiara who listened to me during our dinners and consoled me when I was disappointed and discouraged.

The last thanks go to my Italian colleagues Irene and Fabio. Our business calls to share mutual misfortunes were a good moment for discussion.